NASA CONTRACTOR REPORT

NASA-CR-295

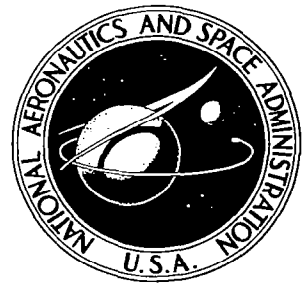

THIN SHEET IMPACT

by C. J. Maiden, A. R. McMillan, and R. E. Sennett III

Prepared under Contract No. NAS 9-3081 *by*
GENERAL MOTORS CORPORATION
Santa Barbara, Calif.
for

NATIONAL AERONAUTICS AND SPACE ADMINISTRATION • WASHINGTON, D. C. • SEPTEMBER 1965

THIN SHEET IMPACT

By C. J. Maiden, A. R. McMillan,
and R. E. Sennett III

Prepared under Contract No. NAS 9-3081 by
GENERAL MOTORS CORPORATION
Santa Barbara, Calif.

for

NATIONAL AERONAUTICS AND SPACE ADMINISTRATION

For sale by the Clearinghouse for Federal Scientific and Technical Information
Springfield, Virginia 22151 – Price $3.00

ABSTRACT

Results are presented from a theoretical and experimental program to investigate the shielding necessary to protect a spacecraft from meteoroid impact damage. A previous study shows that heating effects from impact can melt or vaporize debris that passes through a thin shield. The momentum loading of this debris was measured and the results applied to calculating the response of the second sheet, using numerical shell analysis techniques. Shielding calculations and experiments predict that a first sheet of 0.20-mm aluminum and a second sheet of 1.40-mm 7075-T6 aluminum, 5.08 cm apart, will have a probability of 0.999 of no damage on an Apollo mission.

CONTENTS

	Page
ABSTRACT	iii
ILLUSTRATIONS	vii
INTRODUCTION	1
INTERACTION OF A PARTICLE WITH A SHIELD	2
Theoretical Model	3
Heating Effects due to Impact	3
The Effect of Impact Velocity	12
INTERACTION OF DEBRIS WITH A SHIELDED TARGET – THEORETICAL	19
Preliminary Experiments	19
Theory of Failure of a Target Due to Gross Deformation	21
The Strip Approximation	24
The Effect of Span	32
Complete Results for Particles with a Diameter of 3.2 mm	32
The Effect of Particle Size	38
The Effect of Spacing	38
The Effect of Pre-Tensioning the Backup Sheet	45
Extensions of the Strip Approximation	45
INTERACTION OF DEBRIS WITH A SHIELDED TARGET – EXPERIMENTAL	48
Momentum Multiplication	48

CONTENTS (Continued)

	Page
Experimental Check of Predictions for a 1.02-mm Aluminum Particle at 30.4 km/sec	51
Spalling Experiments	53
DISCUSSION AND CONCLUSIONS	55
REFERENCES	57

ILLUSTRATIONS

Figure		Page
1a	Wave Pattern in Projectile and Shield Soon After Impact	4
1b	Wave Pattern After Reflection of Shock from Bottom of Shield	4
2	Pressure-Volume Curve	5
3a	Effect of Shield Melting Temperatures, Front of Targets	8
3b	Effect of Shield Melting Temperatures, Rear of Targets	9
4	X-Rays of Impacts of Nickel, Copper, and Cadmium Shields	10
5	Total Penetration vs Impact Velocity	13
6	Total Penetration vs Shield Thickness	15
7	Optimum Shield Thickness vs Velocity – Aluminum Shield and Projectile	16
8	Optimum Shield Thickness vs Velocity – Cadmium Shield and Projectile	18
9	Effect of Backup Thickness	20
10	Framing Camera Sequence of Backup Failure	22
11a	Response of Explosively Loaded 6061-T6 Aluminum Beam	25
11b	Idealized Elastic Perfectly Plastic Stress-Strain Curve for 6061-T6 Aluminum	26
12a	Response of Explosively Loaded 1010 Steel Beam	27
12b	Idealized Strain Rate Behavior for 1010 Steel	28

ILLUSTRATIONS (Continued)

Figure		Page
13	Strip Approximation	29
14a	Centerline Displacement vs Time for 3.2-mm Aluminum Sphere – 0.8-mm Backup	30
14b	Centerline and Edge Strain vs Time for 3.2-mm Aluminum Sphere – 0.8-mm Backup	31
15a	Centerline Displacement vs Time for 3.2-mm Aluminum Sphere – 1.6-mm Backup	33
15b	Centerline and Edge Strain vs Time for 3.2-mm Aluminum Sphere – 1.6-mm Backup	34
16a	Centerline Displacement vs Backup Thickness at 200 Microseconds for 3.2-mm Aluminum Sphere	35
16b	Centerline Strain vs Thickness at 200 Microseconds for 3.2-mm Aluminum Sphere	36
16c	Edge Strain vs Thickness at 200 Microseconds for 3.2-mm Aluminum Sphere	37
17	Backup Thickness vs Velocity for 3.2-mm Aluminum Sphere	39
18	Backup Thickness vs Velocity for 1.6-mm Aluminum Sphere	40
19	Backup Thickness vs Velocity for 1.02-mm Aluminum Sphere	41
20	Backup Thickness vs Particle Diameter to Prevent Yield	42
21	Backup Thickness vs Particle Diameter to Prevent Fracture	43
22	Backup Thickness vs Spacing for 1.02-mm Aluminum Sphere Impacting at 30.4 km/sec	44
23	Centerline Displacement vs Time – Pre-Tensioned Beam	46

ILLUSTRATIONS (Continued)

Figure		Page
24	Backup Thickness vs Pre-Tension Stress	47
25	Momentum Multiplication vs Velocity	49
26	Momentum Multiplication vs Shield Thickness	50
27	Backup Targets – Simulated Apollo Impacts	52

INTRODUCTION

The results presented in this paper represent an extension of the work in thin sheet impact presented by one of the authors[1] at the Sixth Hypervelocity Impact Symposium. Complementary theoretical and experimental techniques were used, with emphasis on protecting space vehicles against meteoroids.

Although our present knowledge of meteoroids is limited,[2] about 90 percent of these particles are believed to be of cometary origin and to have the composition of stone.[3] Estimates of the density of meteoroids[3-5] have ranged from 0.05 to 3 gm/cm^3, with the latest estimate being Whipple's value of 0.44 gm/cm3.[4]

The velocities of meteoroids relative to earth range from 11 to 72 km/sec. The lower limit is the velocity a particle would attain if it started from rest relative to earth and fell several earth radii to the sensible atmosphere. The upper limit is the maximum relative velocity of a collision between the earth and a body in the solar system. Thus, the relative impact velocities of interest to spacecraft designers range from a few kilometers per second to about 80 km/sec.

Because of the general uncertainty in meteoroid properties, NASA has seen fit to publish an Engineering Criteria Bulletin[6] concerning the meteoroid environment to be used for spacecraft design. The environment is as follows:

(a) The isotropic flux-mass relationship for sporadic meteoroids is given by

$$\text{Log}_{10}N = -1.34 \log_{10} m - 10.423 \qquad (1)$$

where N is the number of impacts per square foot per day above mass m in grams.

(b) The density of meteoroids is 0.5 gm/cm^3 for all particle sizes.

(c) The average geocentric velocity is 30 km/sec for all particle sizes.

(d) The anisotropic flux during a shower is given by

$$\text{Log}_{10}N = -1.34 \log_{10} m - 2.68 \log_{10} V - 6.465 + \log_{10} F$$

where V is the geocentric velocity of the meteoroid stream (km/sec), and F is the ratio of accumulative meteoroid stream flux to the sporadic meteor flux.

The isotropic flux relationship (Eq. 1) can be used to calculate the critical meteoroid mass for a specific mission in space.[2] For the Apollo service module with a surface area of approximately 51 square meters, a 0.999 probability of no puncture, and a mission time of 14 days, protection should be provided against meteoroids of mass up to 1.48×10^{-3} grams. This mass corresponds to a meteoroid with a diameter of 1.78 mm and a density of 0.5 gm/cm^3, or an aluminum particle with a diameter of 1.02 mm.

Unfortunately, it is difficult to simulate meteoroids in the laboratory. Hypervelocity accelerators are limited to velocities below about 10 km/sec; and it is difficult to launch particles of meteoroid density even up to these velocities. For these reasons, this study has been directed towards understanding the physics of the interaction of a hypervelocity particle with a shielded structure. With this understanding, the results can be extrapolated with confidence to cover the range of velocity and particle density relevant to meteoroids.

INTERACTION OF A PARTICLE WITH A SHIELD

The conclusions reached concerning this subject at the time of the Sixth Hypervelocity Impact Symposium[1] can be summarized as follows:

(a) A shield is effective because it can fracture a hypervelocity particle, spreading its fragments and reducing their velocity below that of the original particle. As a shield is made thinner, its effectiveness at a given velocity is reduced because the spread of fragments is reduced, and fragment velocities tend to approach the velocity of the original particle. In addition, for a given impacting particle, the effectiveness of a shield in fracturing the particle increases with increasing impact velocity.

(b) To a first approximation, shields of different materials but of equal weight are equally effective.

(c) The effectiveness of a shield is not affected by the strength of the shield material at impact velocities above about 4 km/sec.

One factor that was not fully appreciated at the time of the Sixth Symposium was the importance of heating effects in determining the effectiveness of a shield. This and other results of subsequent work are presented.

Theoretical Model

Consider a cylinder impacting a thin shield at hypervelocity. The estimated wave pattern shortly after impact is shown schematically in Fig. 1. Two shock waves S_1 and S_2 have propagated away from the interface I, and, because the projectile is finite in diameter, rarefaction waves R_1 and R_2 have been transmitted towards the axis of symmetry. Also, the formation of these rarefactions has resulted in the ejection of both projectile and shield material in a rearward direction.

Now consider the situation shortly after the shock S_2 has reflected from the back face of the shield (Fig. 1b). In order to satisfy the boundary condition of zero pressure, the shock is reflected as a rarefaction wave R_3. The resultant particle velocities behind R_3 produce the profile of the back face of the shield as shown. As the process continues, the bubble grows through the addition of material from the shield and projectile.

From a physical viewpoint the rarefactions R_1, R_2, R_3, and R_4, generated to satisfy boundary conditions, can be regarded as tension waves; hence, fracture will occur if the net tensile stress at any point in the projectile or shield exceeds the fracture stress. In addition, rarefactions will be produced to satisfy boundary conditions at any new fracture surfaces, and these rarefactions can lead to further fractures. Thus, the whole process of fracture of a projectile and a thin shield can be interpreted as a multiple-spalling phenomenon which starts at the free surfaces.

Heating Effects Due to Impact

An examination of Fig. 1 shows that during the impact process each element of the projectile and the shield is first shocked to some pressure, and is then brought back to ambient pressure by rarefaction waves. This process is represented on a pressure-volume plot in Fig. 2. Each element of material starts off at some initial density ρ_0 and is compressed on the Hugoniot (points 1–2) to some pressure P_H by

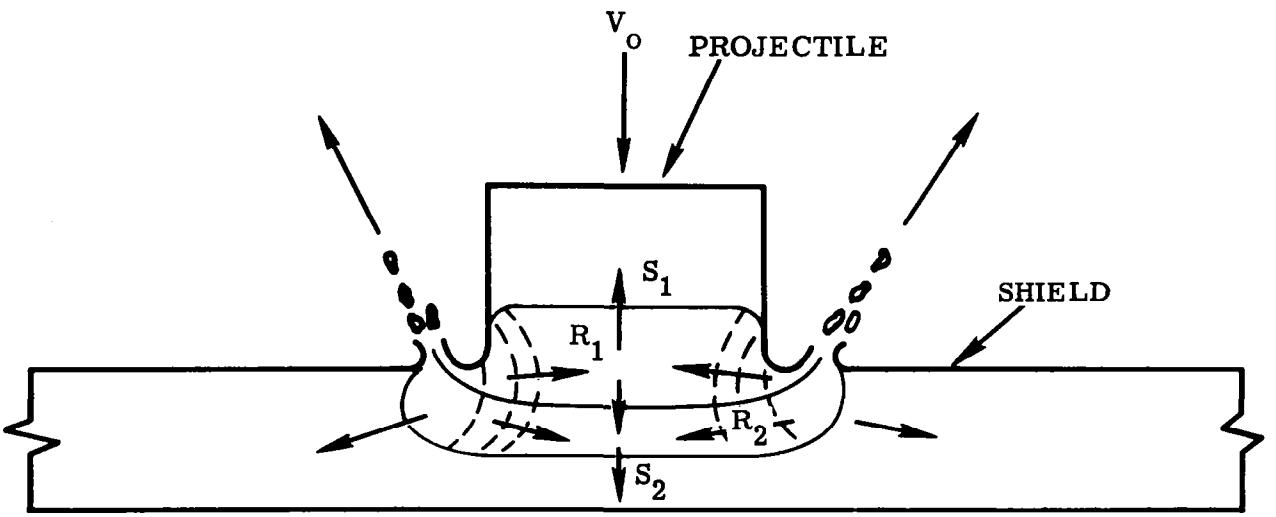

Fig. 1a Wave Pattern in Projectile and Shield Soon After Impact

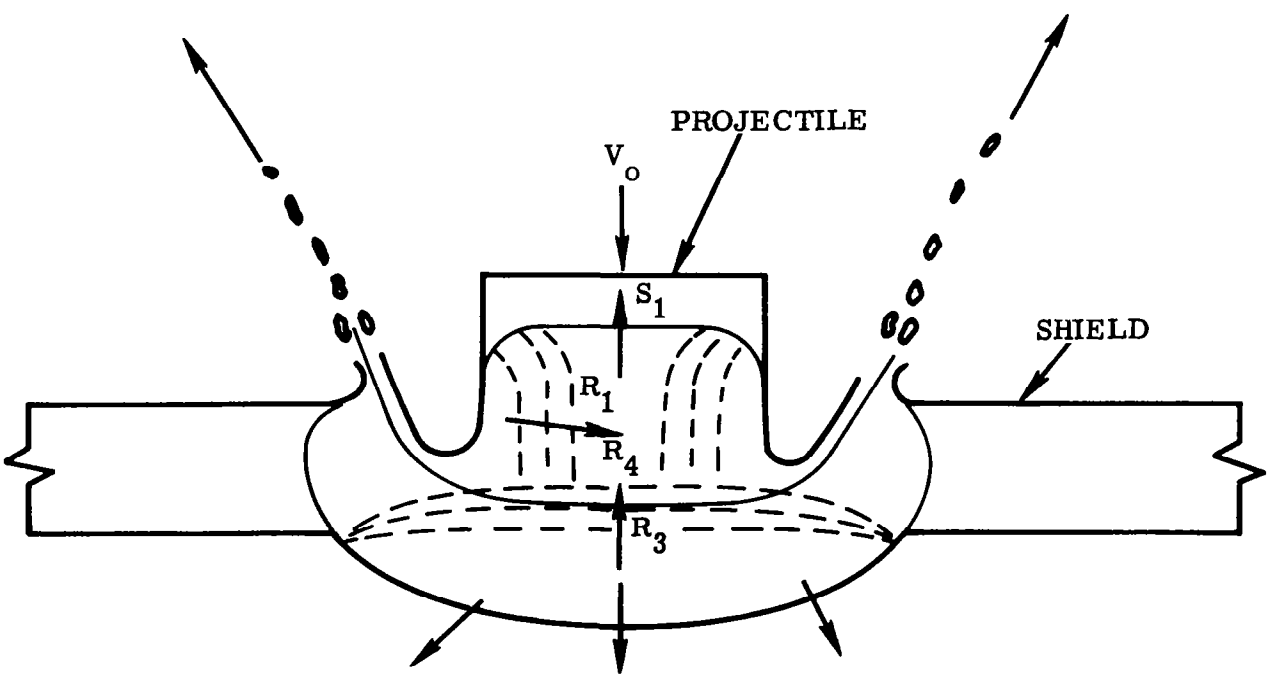

Fig. 1b Wave Pattern After Reflection of Shock from Bottom of Shield

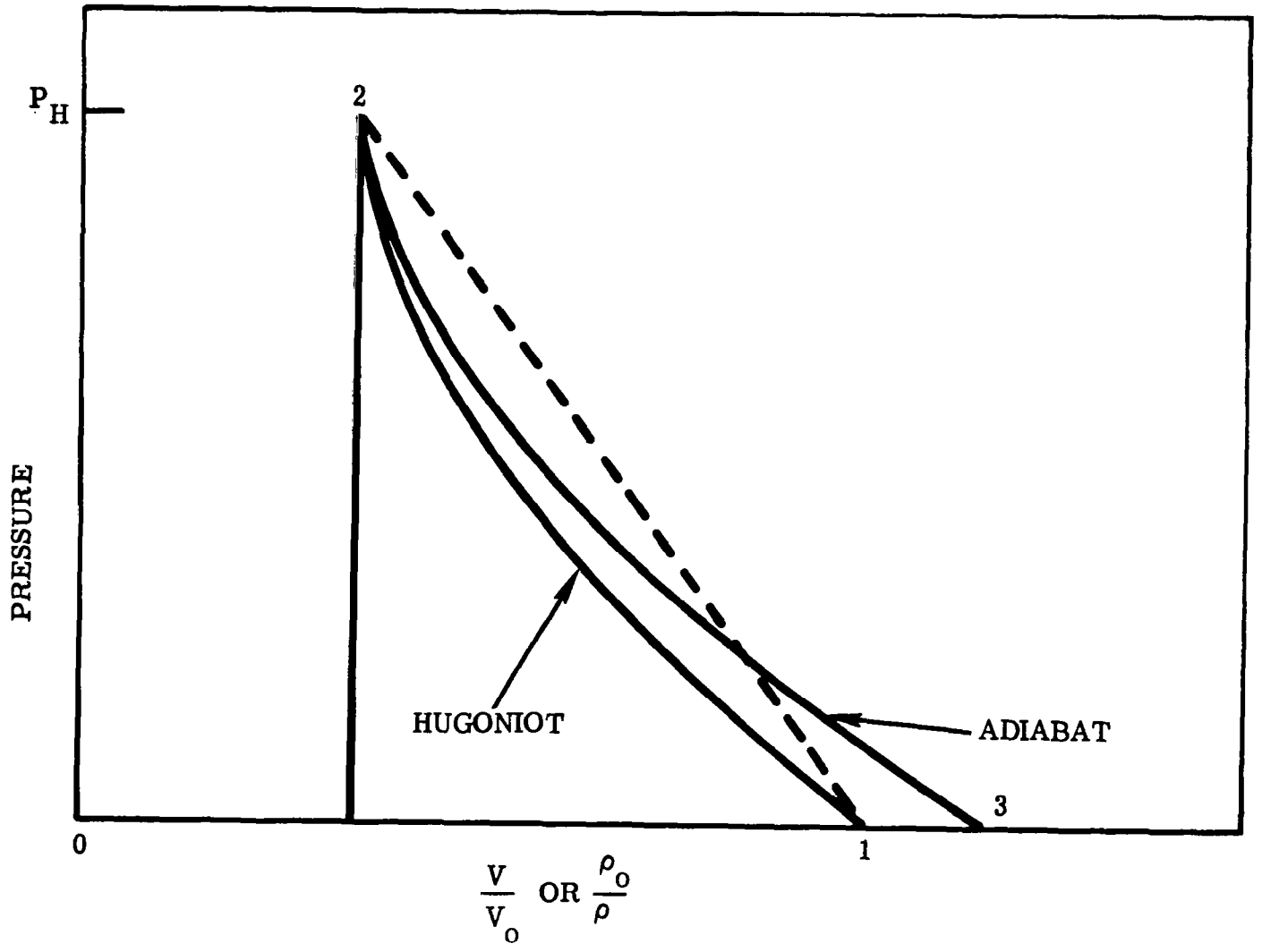

Fig. 2 Pressure-Volume Curve

a shock wave. The material is then brought back to ambient conditions adiabatically (points 2–3) by rarefaction waves. The initial shocking process is nonisentropic, whereas the release process is isentropic. Thus, the entropy of the material has been increased by the impact process. In other words, the element of material in its final state will be heated. The specific internal energy e_H of the shock-compressed material is equal to the area of the dashed triangle $P_H/2\ (v_o - v_H)$ in Fig. 2, whereas the energy that is returned by the material in pressure-volume work on expansion is the area under the adiabat. The area under the adiabat is less than the area under the triangle, and the difference between the two is proportional to the residual heat left in the element. Shocks of low strength will leave the material heated but in the solid state. As the shock strength is increased the entropy excess, which increases rapidly, can lead to melting, heated liquid, vaporization, or super-heated vapor in the final state.

A more complete discussion of this phenomenon has been made by Olshaker and Bjork[7] and McQueen and Marsh.[8] These workers have calculated, for a number of materials, the values of shock pressure sufficient to cause incipient melting, complete melting, and vaporization when the materials are returned to atmospheric pressure. Some estimated values of these pressures are tabulated in Table I for materials of interest here. Note that, in many cases, appropriate shock pressures for the above changes are not available. Note also that the above heating effects will be enhanced at low velocities by material viscosity.

Table I

SHOCK HEATING EFFECTS

Material	Melting Temperature (°C)	Vaporization Temperature (°C)	Pressure to Cause Incipient Melting (Mbars)	Pressure to Cause Complete Melting (Mbars)	Pressure to Cause Vaporization (Mbars)
Aluminum	660	2,057	0.6	0.9	-
Cadmium	321	767	0.4	0.46	0.8
Copper	1,083	2,336	1.4	>1.5	-
Gold	1,063	2,600	1.5	1.6	-
Iron	1,535	3,000	-	2.0	-
Lead	327	1,620	0.3	0.35	1.0
Magnesium	651	1,107	-	-	-
Nickel	1,455	2,900	>1.5	-	-
Titanium	1,800	>3,000	>1.1	-	-

It is considered that the above heating effects are important in determining the size of particles in the bubble. If the final debris is in the solid state, the size of spall fragments will decrease with increasing temperature because of a decrease in fracture strength. If the material is molten, then only surface tension forces need be overcome to create droplets. These forces, and hence droplet size, will decrease as the liquid becomes hotter. Finally, if the heating effects are great enough, the debris becomes vapor.

Experimental verification of the importance of such effects is shown by the results of three series of ballistic range firings using nickel, copper, and cadmium shields. These materials were chosen because they have almost identical densities but very different thermal properties. In all cases the protected targets were 6.4-mm 2024-T3 aluminum plates spaced 5.08 cm behind the shields, and the shield thickness was 1.016 mm.

The first series of tests used 6.35-mm aluminum spheres at 4.16 km/sec. The targets from these tests are shown in the top rows of Fig. 3a and 3b, where frontal damage to the targets is immediately seen to decrease in the shield order of nickel, copper, and cadmium. Tables I and II help explain this result. It is seen that at 4.16 km/sec the maximum impact pressure (calculated by the method described in Ref. 1) is sufficiently high to melt only the cadmium debris from the shield, but not the copper or nickel fragments. As a result, the frontal damage to the backup target with a cadmium shield is reduced significantly because the molten cadmium particles are extremely small, whereas frontal damage to the targets with the copper and nickel shields is caused by the larger solid fragments (see top row of Fig. 4). Of course, debris from the aluminum projectile also causes damage to the backup target; however, the impact pressures for the three shield materials are such that this damage is expected to be least with the nickel, next with the copper, and greatest with cadmium. Thus, the differences in the damage in Fig. 3 are directly attributable to the state of the shield debris.

In the second series of tests, 6.35-mm aluminum spheres were impacted at 7.31 km/sec. Table II shows that the maximum impact pressures generated in these tests are sufficient to completely melt some parts of the aluminum projectiles, vaporize the cadmium,and just cause incipient melting of the

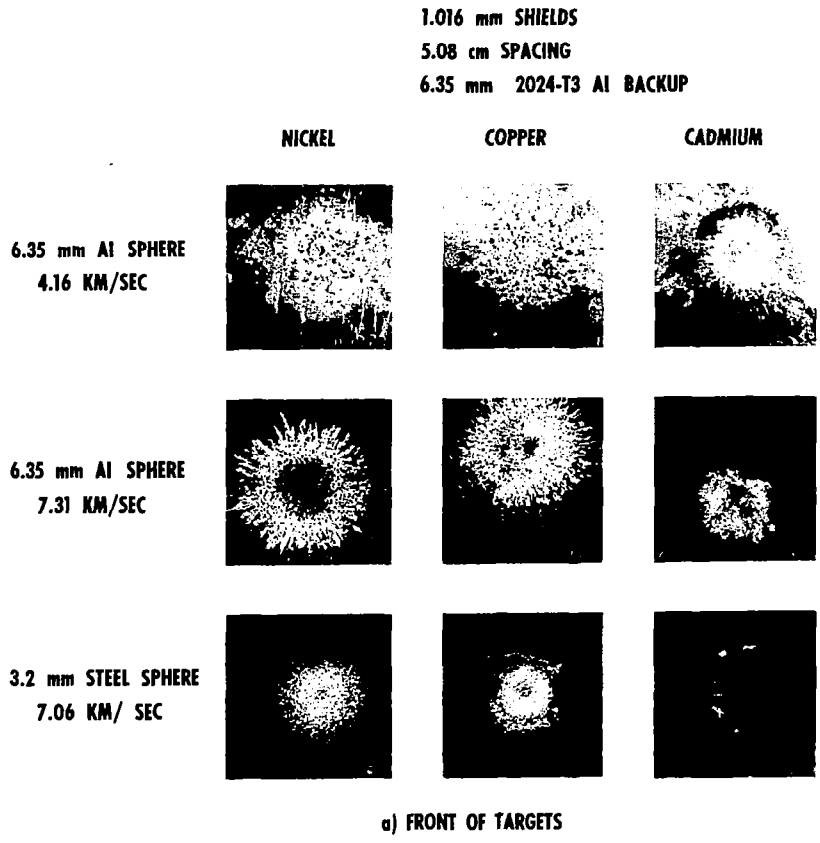

Figure 3a Effect of Shield Melting Temperatures, Front of Targets

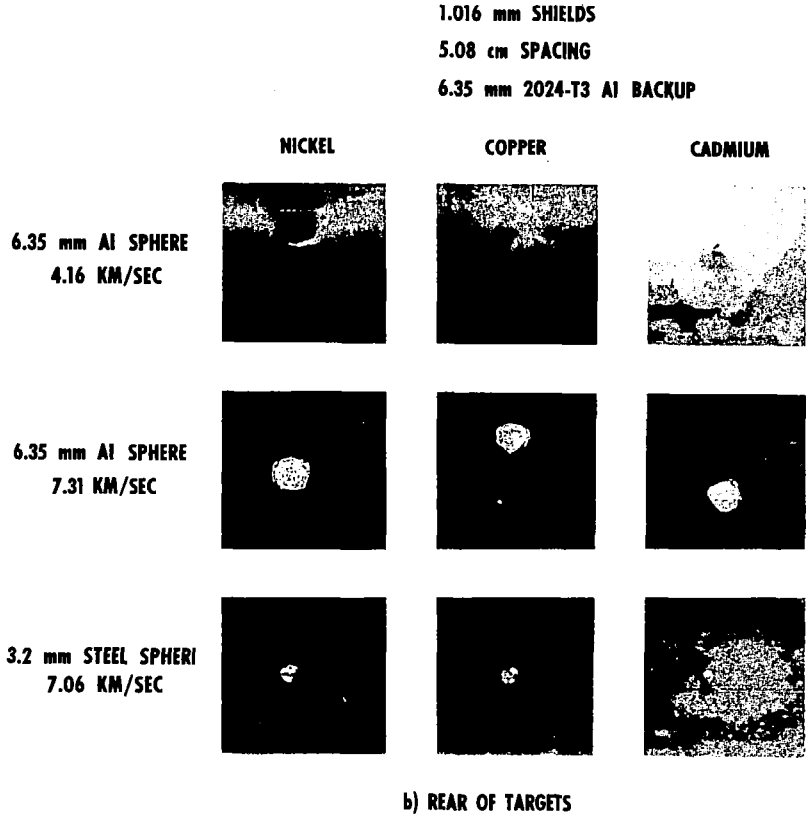

Figure 3b Effect of Shield Melting Temperatures, Rear of Targets

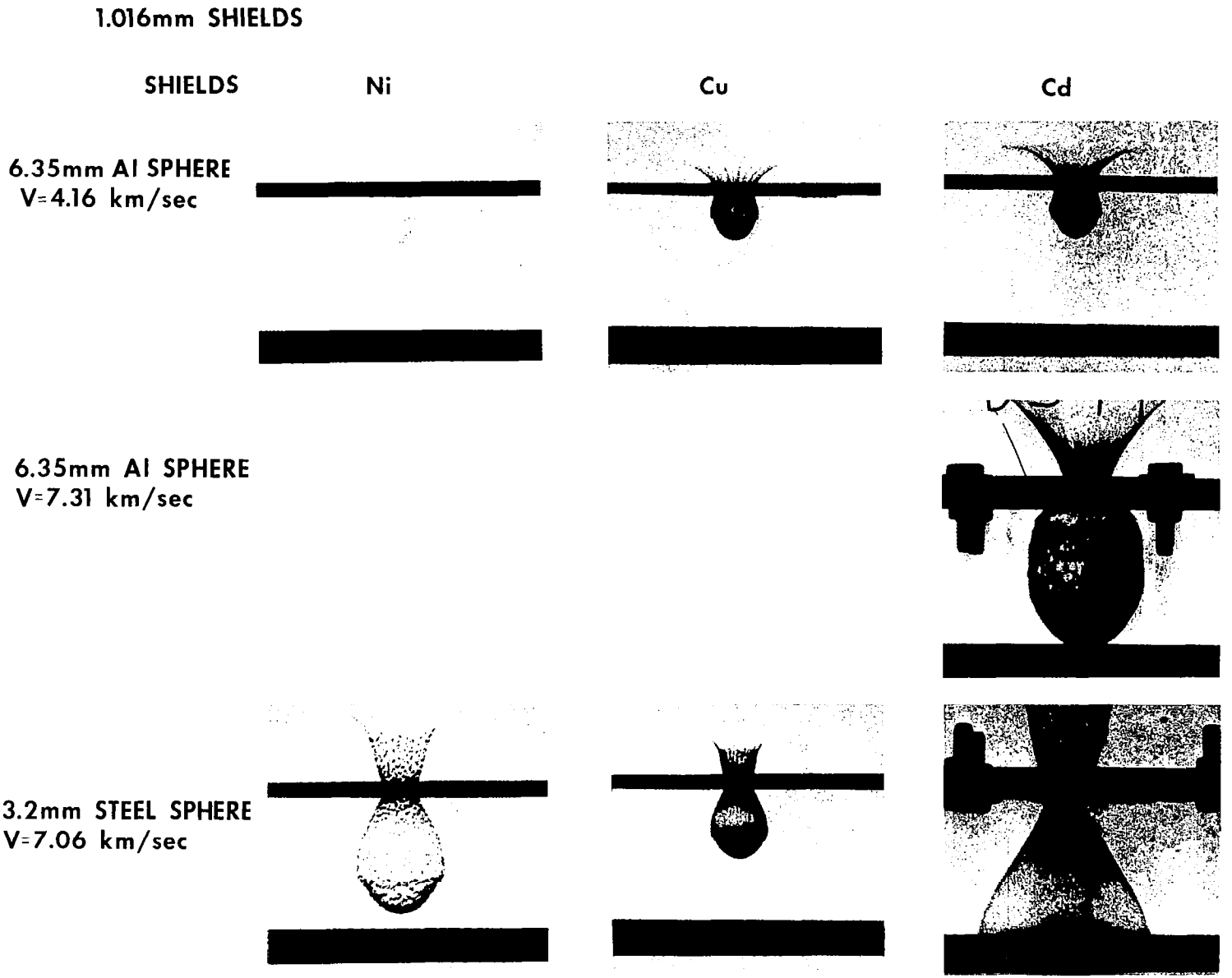

Figure 4 X-Rays of Impacts of Nickel, Copper, and Cadmium Shields

Table II

CHARACTERISTICS OF IMPACTS
IN Cd, Cu, Ni

Projectile	Velocity (km/sec)	Target	Pressure (mbars)
Aluminum	4.2	Cd	0.67
		Cu	0.72
		Ni	0.75
Aluminum	7.3	Cd	1.50
		Cu	1.57
		Ni	1.67
Steel	7.1	Cd	2.60
		Cu	2.90
		Ni	3.05

copper. The targets (second rows of Fig. 3) tend to confirm these theoretical predictions. For instance, a "splash" of aluminum can be observed on all three targets. In addition, the frontal damage to the target with a cadmium shield is almost negligible, whereas pitting on the target with a nickel shield suggests that the nickel fragments are not molten upon impact. The X-ray for the cadmium shield, shown in Fig. 4 for this series of tests, indicates that the debris in the bubble exists in states other than solid fragments.

In the third series the maximum impact pressure (Table II) was increased even further than in the first two series. In these tests, 3.2-mm steel spheres were fired at 7.06 km/sec. The targets are shown in the bottom rows of Fig. 3, and corresponding X-rays are shown in the bottom row of Fig. 4. Once again the cadmium shield is the best; but, now the copper is shocked to a pressure sufficient to become molten, so the cadmium and copper shields are almost equally effective. Also, both the X-ray and the target with the nickel shield indicate that the nickel debris is still solid. In the X-ray for the cadmium shield it is difficult to distinguish any particulate debris in the bubble.

Two points of interest from these tests should be emphasized. The first is that the debris from both the projectile and shield cause damage to the backup target. The debris

from the shield can be particularly damaging because a large portion of it will travel at near the initial impact velocity; hence, the state of the debris from the shield is very important in determining the depth of penetration in the backup target. The second point comes from examining the rear of the backup targets (Fig. 3b); these show that the spall-producing load is essentially independent of the state of the material in the bubble.

The Effect of Impact Velocity

The question of how the effectiveness of a shield varies with impact velocity is of particular interest to the spacecraft designer because laboratory test velocities are limited to about 10 km/sec. A series of tests was conducted to shed further light on this problem.

In these tests, the projectiles were 3.2-mm aluminum spheres, the spacing between shield and target was 5.08 cm, and the backup targets were effectively semi-infinite blocks of 2024-T3 aluminum. The tests were conducted over a range of impact velocities. The shields were 2024-T3 aluminum, 0.13, 0.40, 0.81, 1.22, and 1.62 mm thick.

Results of some of the tests are shown in Fig. 5, where total depth of penetration p_T (shield thickness plus depth of penetration in the target) has been plotted against impact velocity for shield thicknesses of 0.13, 0.40, and 1.22 mm. Also shown in this figure is the curve for penetration into semi-infinite targets taken from Ref. 1. This latter curve can be looked upon as the result for a shield that is very thick or negligibly thin. With the former, the projectile will not penetrate; with the latter, the shield will be completely ineffective.

Results show that up to velocities of 2 to 4 km/sec the total depth of penetration of a shield is slightly more than the penetration into an unprotected target. At these lower velocities, it is apparently easier to perforate the shield than to penetrate an equal distance into a semi-infinite target. As the impact velocity is increased, however, the shields become more and more effective, because projectile fragmentation is very small until a velocity of 2 to 4 km/sec is reached. As the impact velocity is increased above this region, more uniform and complete fragmentation of the projectile takes place. At about 5 km/sec, incipient melting of some of the

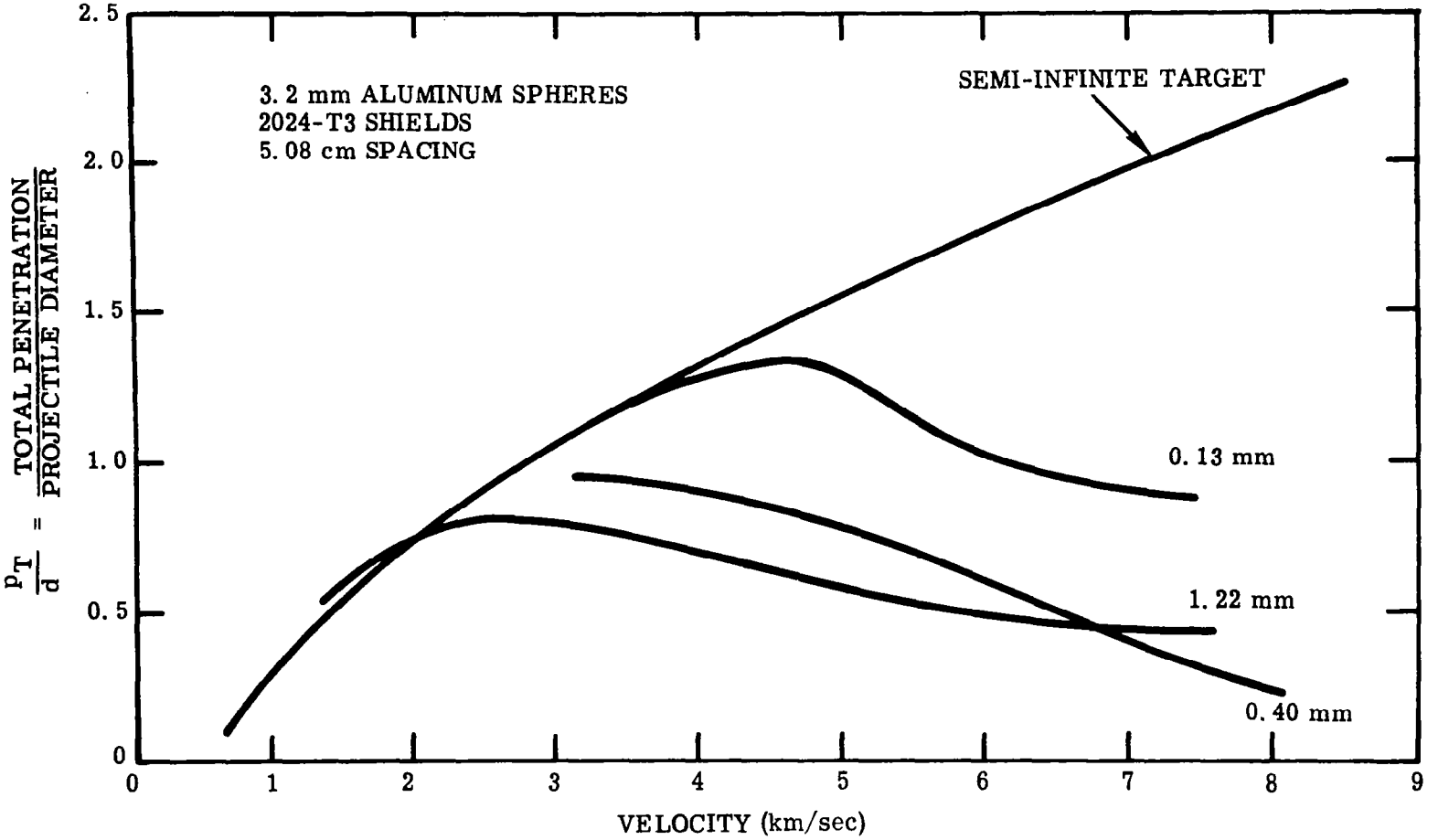

Fig. 5 Total Penetration vs Impact Velocity

aluminum debris occurs, and at 6.5 km/sec complete melting of some of the fragments is expected. As a result, the curves for the 1.62-mm and 1.22-mm shields were found to have almost asymptoted to the shield thickness at 8 km/sec. This indicates that the debris impacting the backup target is so small (due to being molten) that its penetration is negligible. The curves for the other shield thicknesses indicate that, at sufficiently high velocities, they also would asymptote to the shield thickness.

To examine how the optimum shield thickness varies with impact velocity, the total penetration has been plotted as a function of shield thickness at velocities of 4, 6, and 8 km/sec. The results are shown in Fig. 6. Also plotted in this figure is the line corresponding to $p_T = t_S$; i.e., no penetration in the backup target. It is seen that, as the impact velocity increases, the optimum shield thickness decreases. Also, as the impact velocity increases, the total depth of penetration tends towards the shield thickness at lower values of t_S/d.

These last two facts led the authors to consider the following criterion for selection of an optimum shield. It was postulated that an optimum shield would be just thick enough so that the strength of the axial element of the shock S_1 reaching the back of the projectile would be just strong enough to cause eventual melting of this element. Thus, for aluminum, the maximum shock strength at the back of the projectile should be 0.9 megabar. If the shield were thicker than this optimum value, the axial element of the back of the projectile would still become liquid in form but at a higher temperature than the melting temperature. In this case, the size of the droplets, and hence their damaging ability, would be negligibly smaller than the droplets produced with the optimum shield. On the other hand, if the shield were thinner than the optimum value, the central element of the back of the projectile would remain in the solid state and could cause significant damage.

Based on the above criterion and using Fowles' solution,[9] the optimum shield thickness for aluminum impacting aluminum was calculated as a function of impact velocity. The results of the calculations (Fig. 7) clearly show that, based on the present criterion, the optimum shield thickness for minimum total penetration decreases significantly with impact

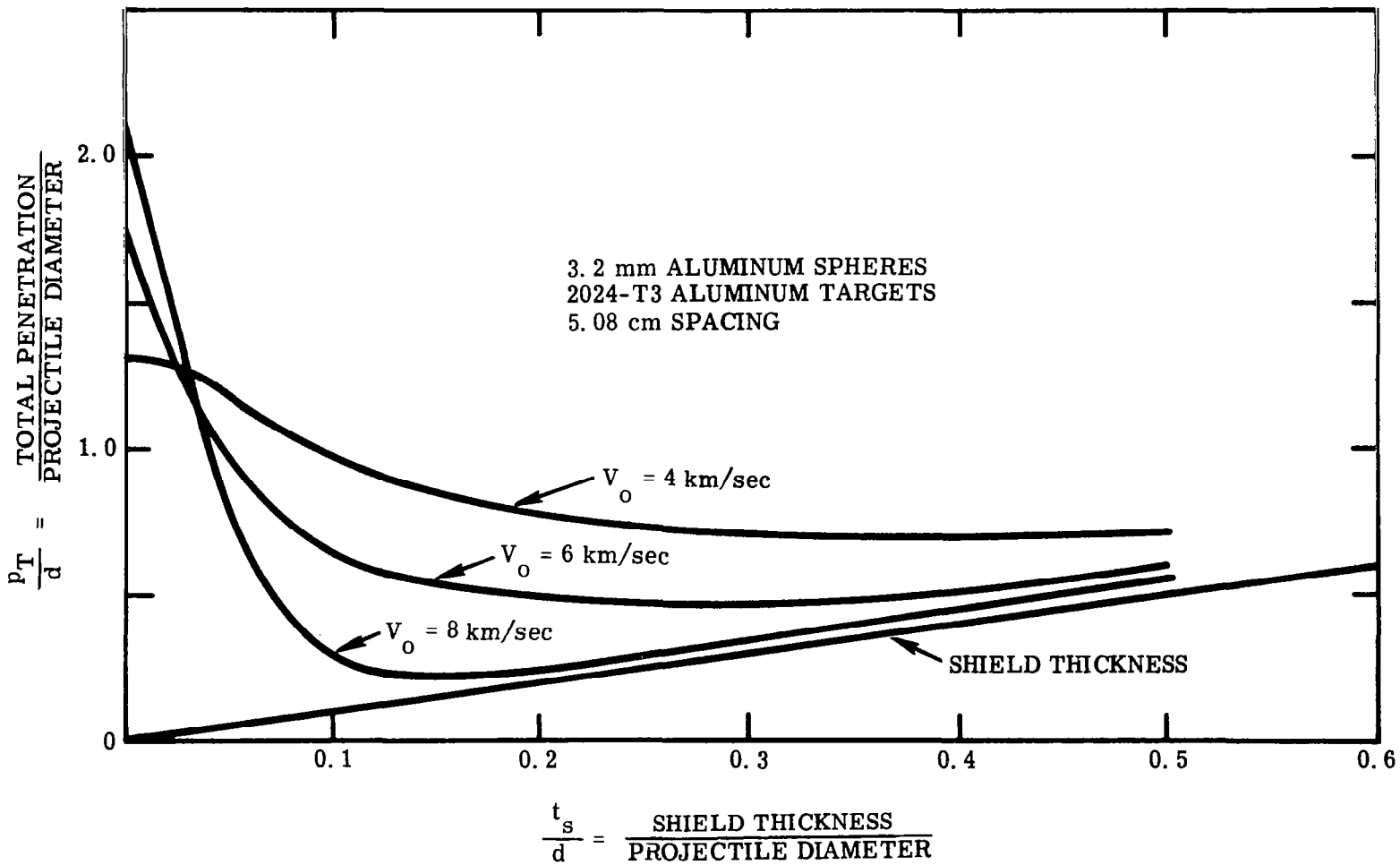

Fig. 6 Total Penetration vs Shield Thickness

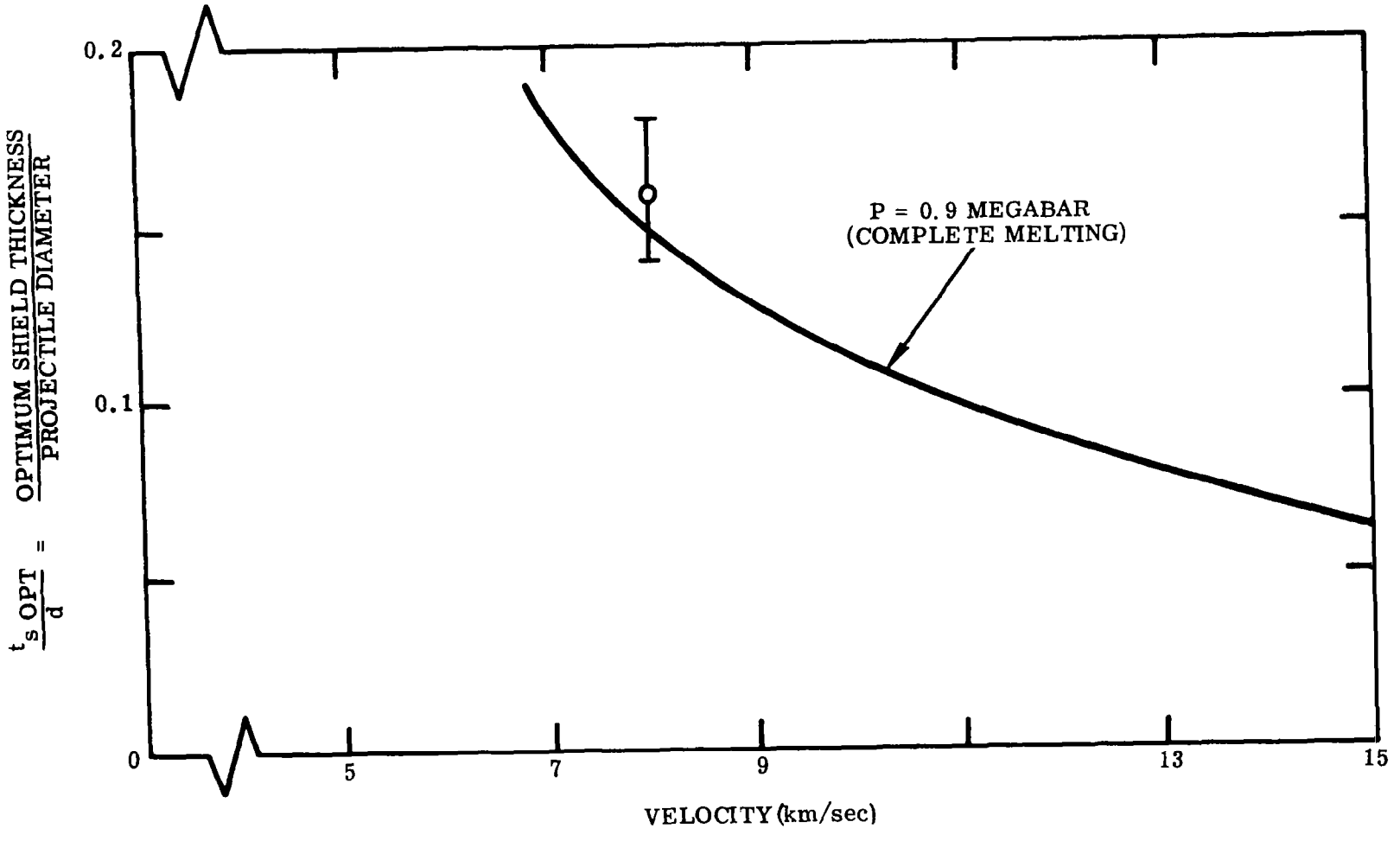

Fig. 7 Optimum Shield Thickness vs Velocity – Aluminum Shield and Projectile

velocity. Figure 7 also shows the experimentally measured optimum at 8 km/sec, and agreement between theory and experiment is good. Unfortunately, melting occurs only at 6.5 km/sec, and the experimental techniques are limited to velocities less than 10 km/sec; thus, the theory is checked only over a limited velocity range.

To extend the comparison of theory and experiment over a greater range of velocities, tests were conducted with cadmium projectiles and shields. Since some of the debris will melt at about 2.3 km/sec, and will vaporize at about 3.8 km/sec, a comparison of theory with experiment can be made over a greater velocity range with cadmium than with aluminum.

In the cadmium tests the projectiles were 3.2-mm spheres, the backup targets were aluminum (2024-T3) plates 6.4 mm thick, and the spacing was 5.08 cm. The experiments were conducted at velocities of 3.0, 3.87, 5.44, 6.55, and 7.3 km/sec. The experimental optima from these tests, together with the theoretical optimum shield thicknesses, are shown in Fig. 8. Note that in this figure theoretical curves are shown corresponding to two criteria for selection of an optimum shield. These criteria correspond to conditions where the axial element of the back of the projectile will end up either just molten or just vaporized.

Several comments can be made concerning the results of such tests.

(a) Large error bars on the experimental points in Fig.8 are necessary because the minima of the penetration curves were not clearly defined. Hence, small errors in measurement have considerable influence on the positions of the minima. Despite this, one can draw the following conclusions: At low velocities there is reasonable agreement between experiment and theory based on the melting criterion; this is not too surprising because no vaporization occurs at velocities below 3.8 km/sec. At higher velocities the experimental points agree more with the theory based on the vaporization criterion. Note that the two criteria for selecting an optimum shield are based on the fact that either melting or vaporization of the axial element of the back of the projectile must occur. When either of these conditions is achieved, some material

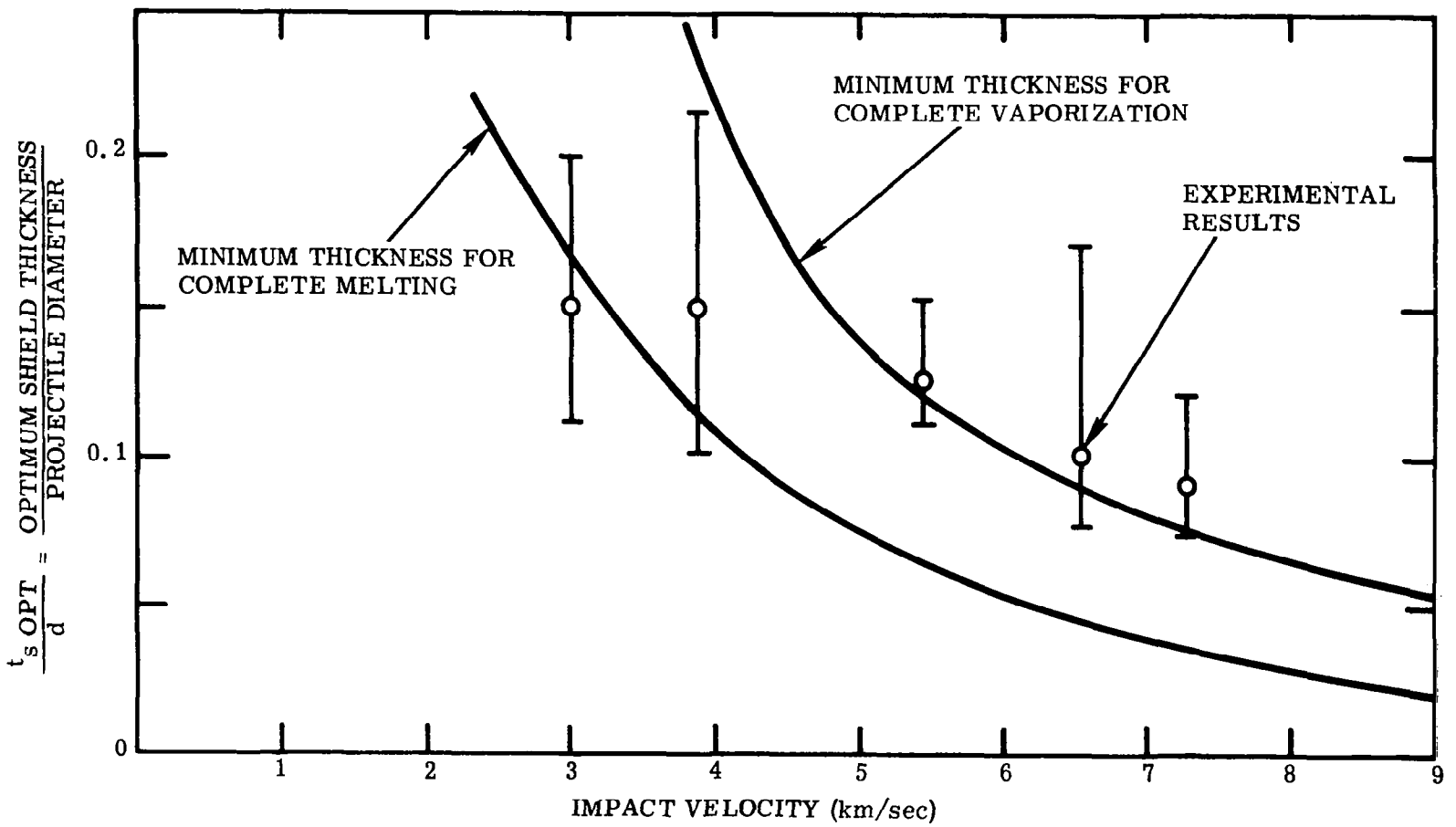

Fig. 8 Optimum Shield Thickness vs Velocity – Cadmium Shield and Projectile

from the sides of the projectile will be in solid form. The experimental results indicate that this debris, although not molten or vaporized, is so small that it is not necessary to use a thicker shield than that based on the relevant criterion. X-rays from the tests support this conclusion.

(b) The backup targets corresponding to the 0.20-mm shields ($t_s/d = 0.064$) showed increased damage from spalling as the impact velocity was increased. This leads to the following important point: The present criterion for selecting an optimum shield gives only the condition for minimum frontal damage ($p_T \longrightarrow t_s$) to a backup target. However, even if the debris impacting such a backup target is in gaseous form, it can still exert a severe impulsive loading that can lead to bending, spalling, or the punching out of a segment of the target. (The next section of this paper concerns itself with this aspect of the problem.)

(c) Recent tests of cylindrical aluminum projectiles impacting shields head-on indicate that the optimum shield criteria above are most applicable to spherical projectiles. With cylinders, the debris coming through the shield spreads out less than the debris from equiweight spherical projectiles; hence, it can form a significant crater in a backup target even though most of the debris is in a molten state. It is thus evident that the optimum shield thickness for a cylindrical projectile will be greater than that for an equivalent sphere; however, the optimum shield thickness is expected to vary with velocity in the manner shown in Figs. 7 and 8.

INTERACTION OF DEBRIS WITH A SHIELDED TARGET – THEORETICAL

Preliminary Experiments

A series of preliminary experiments were made to investigate the types of failure that can result from the collective impact of debris on a shielded structure. In these experiments the projectiles were 3.2-mm aluminum spheres at 8.07 km/sec, the shields were 1100-0 aluminum 0.53 mm thick (near optimum from Fig. 7), the spacing was 5.08 cm, and the backup sheets were 7075-T6 aluminum, 3.2, 1.6, and 0.8 mm thick. Results of the tests (Fig. 9) show that the 3.2-mm backup sheet was not penetrated, although a spall

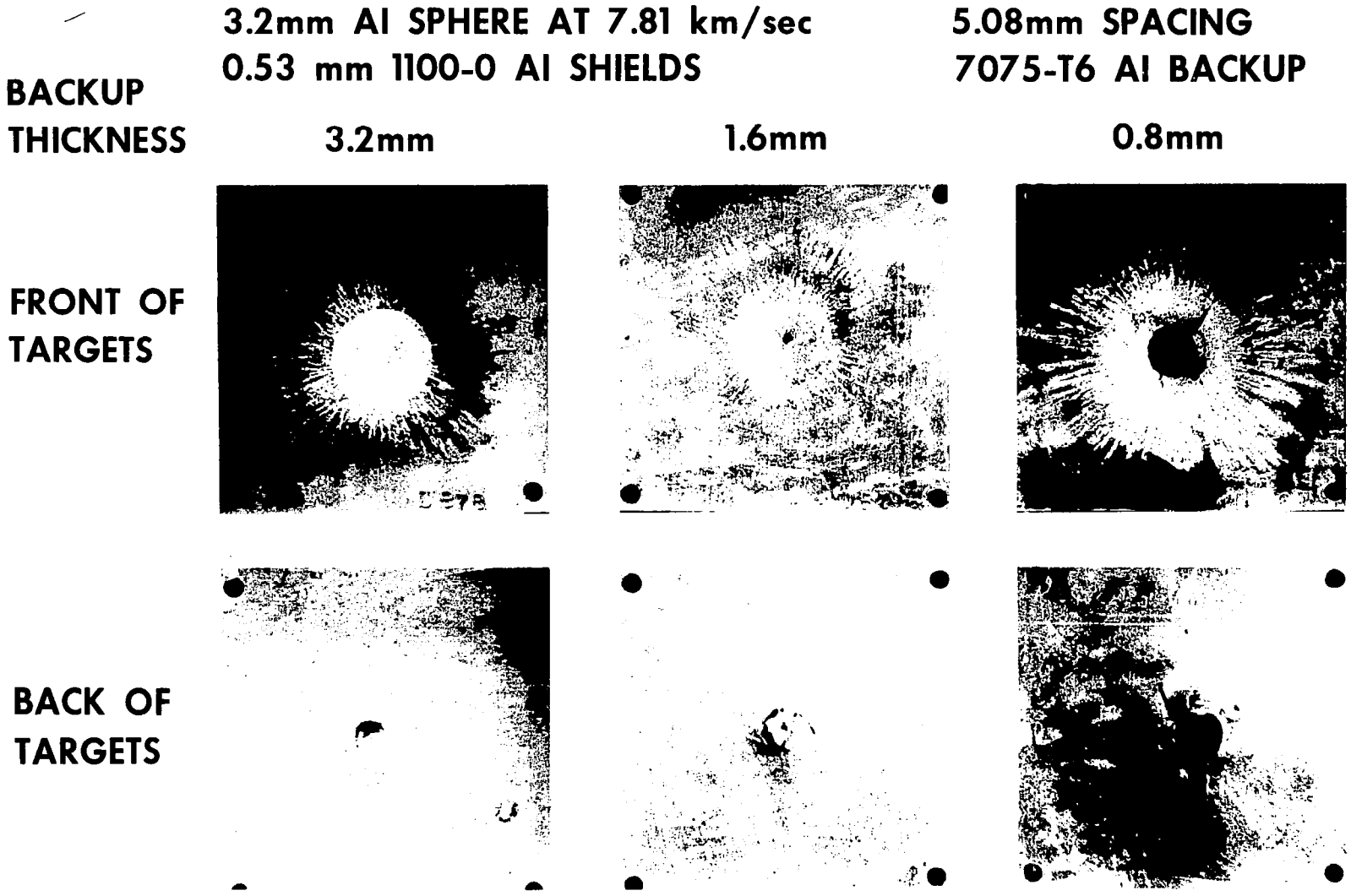

Figure 9 Effect of Backup Thickness

was almost detached; the 1.6-mm sheet has a spall partially detached and exhibits several tensile fractures; and the 0.8-mm target was completely perforated and shows the partial formation of several petals. A Beckman-Whitley framing camera sequence of this last impact (Fig. 10) reveals several interesting features. First, most of the damaging impulse does not occur across the full diameter of the bubble but over a central area with a diameter equal to about half the spacing S (actually about 3/8 S). Second, this central area seems to be fairly uniformly loaded, for a definite step deflection can be seen in the early frames. Third, although a small spall detaches from the target, the main failure mode is tensile failure around the circumference of the loaded area. (Note that failure is not due to shearing as may first be supposed.)

The results above indicate that two failure mechanisms must be considered:

(a) Failure in tension due to the blast-loading effect of the debris impacting the target. Petalling is an example of such a failure.

(b) Failure due to the formation of a spall.

Initial theoretical attention has been given to the first mode of failure.

Theory of Failure of a Target Due to Gross Deformation

To treat this problem theoretically, the magnitude, distribution, duration, etc. of the load applied to the target must first be determined. Then the large deformation dynamic response of the target, taking into account the elastic and plastic behavior of the target material, has to be calculated.

Assumed Loading

The following assumptions have been made:

(a) The load is uniformly distributed over a circular area of diameter equal to one-half the spacing.

(b) The load is applied so quickly that the loaded area is effectively given an initial velocity increment.

(c) The momentum transferred to the loaded area is equal to twice the momentum of the original particle.

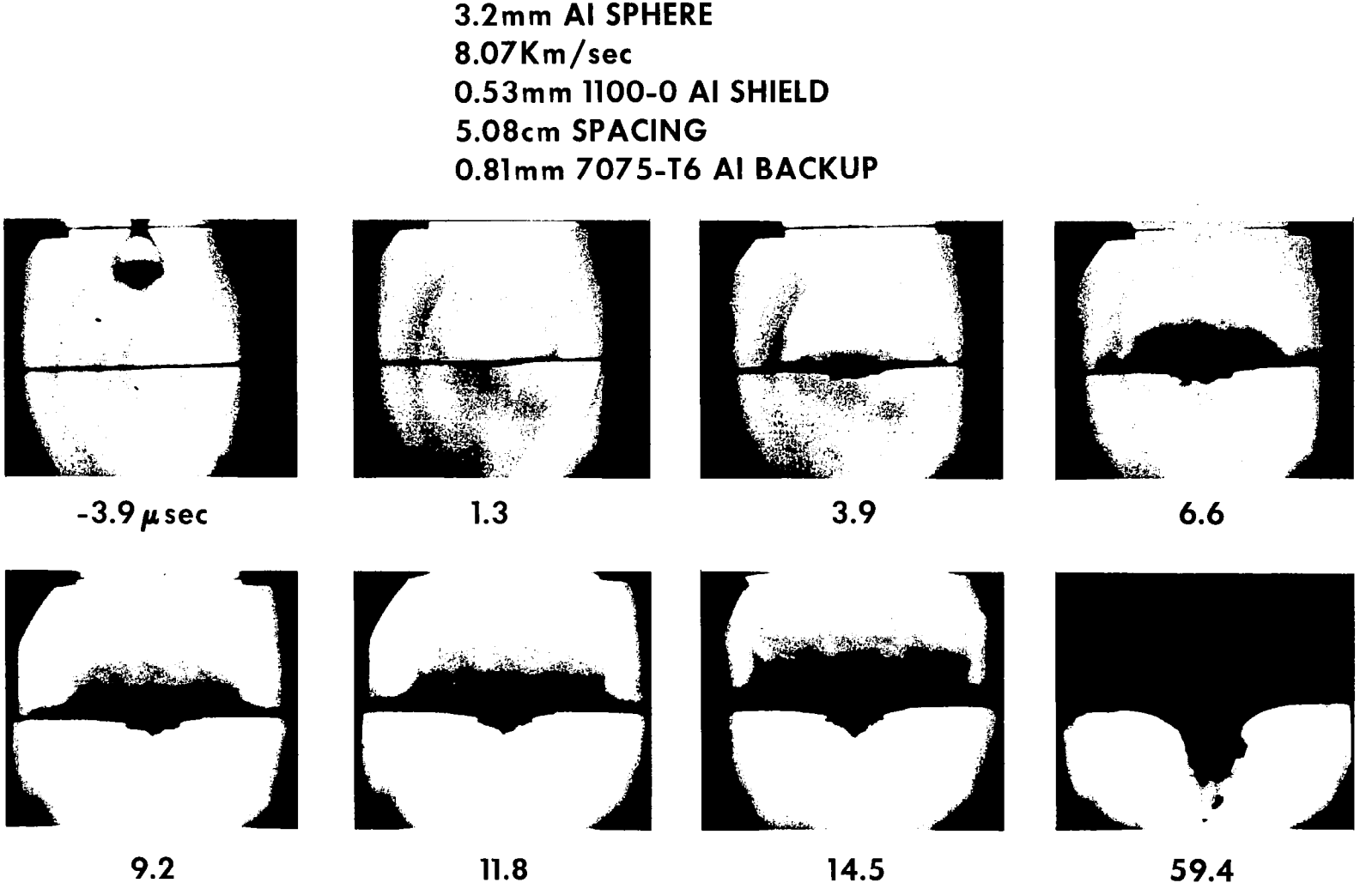

Figure 10 Framing Camera Sequence of Backup Failure

Main justifications for assumptions (a) and (b) come from the results shown in Figs. 9 and 10, whereas a momentum multiplication factor of two, assumption (c), has been chosen for the following reasons: Since the impulsive load applied to a target increases with increasing impact velocity, a spacecraft inner hull must be designed to resist a meteoroid at the maximum expected velocity of 30 km/sec. At this velocity, the majority of the debris coming through the shield will be in gaseous form. Hence, if it is assumed that the momentum of the debris is equal to the momentum of the original particle and that perfectly elastic collisions occur between each gas atom and the target, then the momentum multiplication factor should be two.

Note that the intention has been to use the above assumptions in preliminary calculations while experimental measurements of momentum multiplication, load distribution, etc. are being made. In this way, as better load inputs become available they can be incorporated into the analysis.

Large Dynamic Deformation Analysis

Given the loading, the next part of the problem is to determine the response of the target (assumed to be a thin shell). However, the problem of determining dynamic deformations and stresses in thin shells involves, in general, a complex system of nonlinear differential equations. For these problems that involve both large deflections and plasticity effects, a numerical technique has been developed by Witmer, et al.[10] This technique is based on a finite difference approximation for the original nonlinear differential equations. These finite difference equations are then used to describe an equivalent lumped parameter model. For the timewise step-by-step numerical analysis, the increments in stress resultants and stress couples are determined by idealizing the shell thickness as consisting of n concentrated layers (six layers were used in all the present calculations). Also, the material behavior used to determine the above increments can include elastic, perfectly plastic, elastic-strain hardening, or elastic-strain-hardening strain-rate-sensitive behavior.

The success of this technique is shown in a comparison of theory and experiment for explosively loaded beams.[10] Typical results are shown for a 6061-T6 aluminum beam in

Fig. 11a and for a 1010 steel beam in Fig. 12a. In both cases the agreement between theory and experiment is very reasonable. Note that 6061-T6 aluminum has a low strain rate sensitivity and is assumed to behave in an elastic-perfectly plastic manner (Fig. 11b); whereas 1010 steel has a high strain rate sensitivity, and its assumed behavior is shown in Fig. 12b.

The Strip Approximation

Figure 13 shows the approximation that was first investigated to determine the motion and stresses in the backup sheet. A strip (or beam) of material through the center of the loaded area has been considered, with the argument that the deflections and stresses in the complete plate would be less than those in the strip; hence, any design based on such an approximation would be conservative. Also, since computing time for the strip is much less than for the plate, it was considered worthwhile to first investigate this approximation.

The rear sheet material has been taken as 7075-T6 aluminum. This material has been assumed to behave in an elastic-perfectly plastic manner (see Fig. 11b) with a yield strength σ_o of 46.7×10^8 dynes/cm^2 (70,000 lb/in^2) and a percentage elongation to fracture of 11 percent. The first step is to calculate the initial velocity v_i imparted to the central portion of the strip. From the previous assumptions, this is given by

$$v_i = \frac{32\, M_p\, V_p}{\pi S^2 \rho_b t_b} \tag{2}$$

where M_p and V_p are the mass and velocity of impacting particle, S is the spacing, and ρ_b and t_b are the density and thickness of the backup target. For the initial calculation, the following parameters were used: M_p = mass of 3.2-mm aluminum sphere, V_p = 7.62 km/sec, S = 5.08 cm, and t_b = 0.8 mm. Thus, this case corresponds to one of the preliminary experimental results shown in Fig. 9.

The results of the calculation are shown in Figs. 14a and 14b. The centerline deflection, the tensile strain at the edge of the loaded area, and the tensile strain at the center of the load are shown in these figures. Figure 14a includes the experimental curve of centerline deflection determined from the B&W photos (Fig. 10), indicating good agreement between

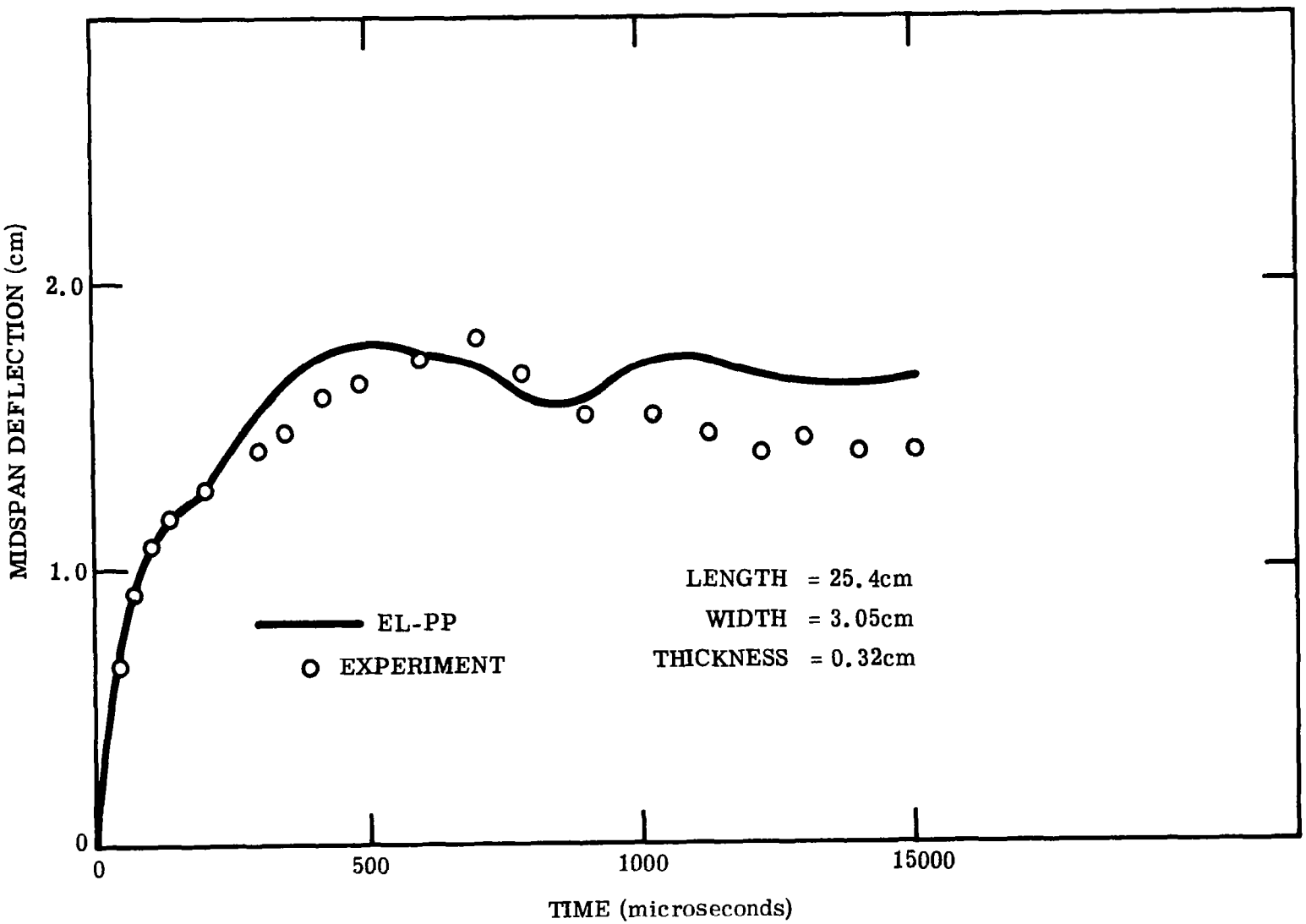

Fig. 11a Response of Explosively Loaded 6061-T6 Aluminum Beam

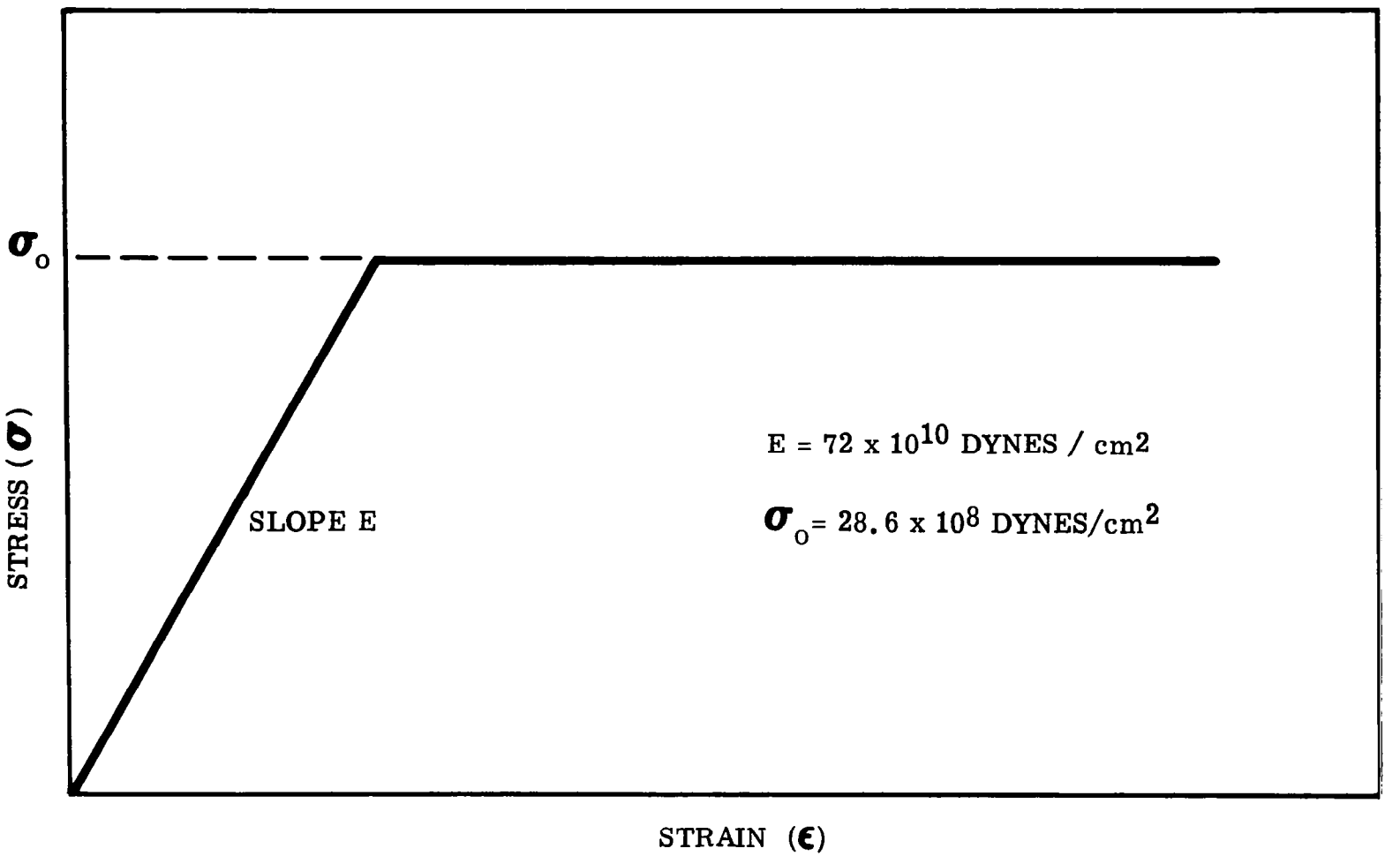

Fig. 11b Idealized Elastic Perfectly Plastic Stress-Strain Curve for 6061-T6 Aluminum

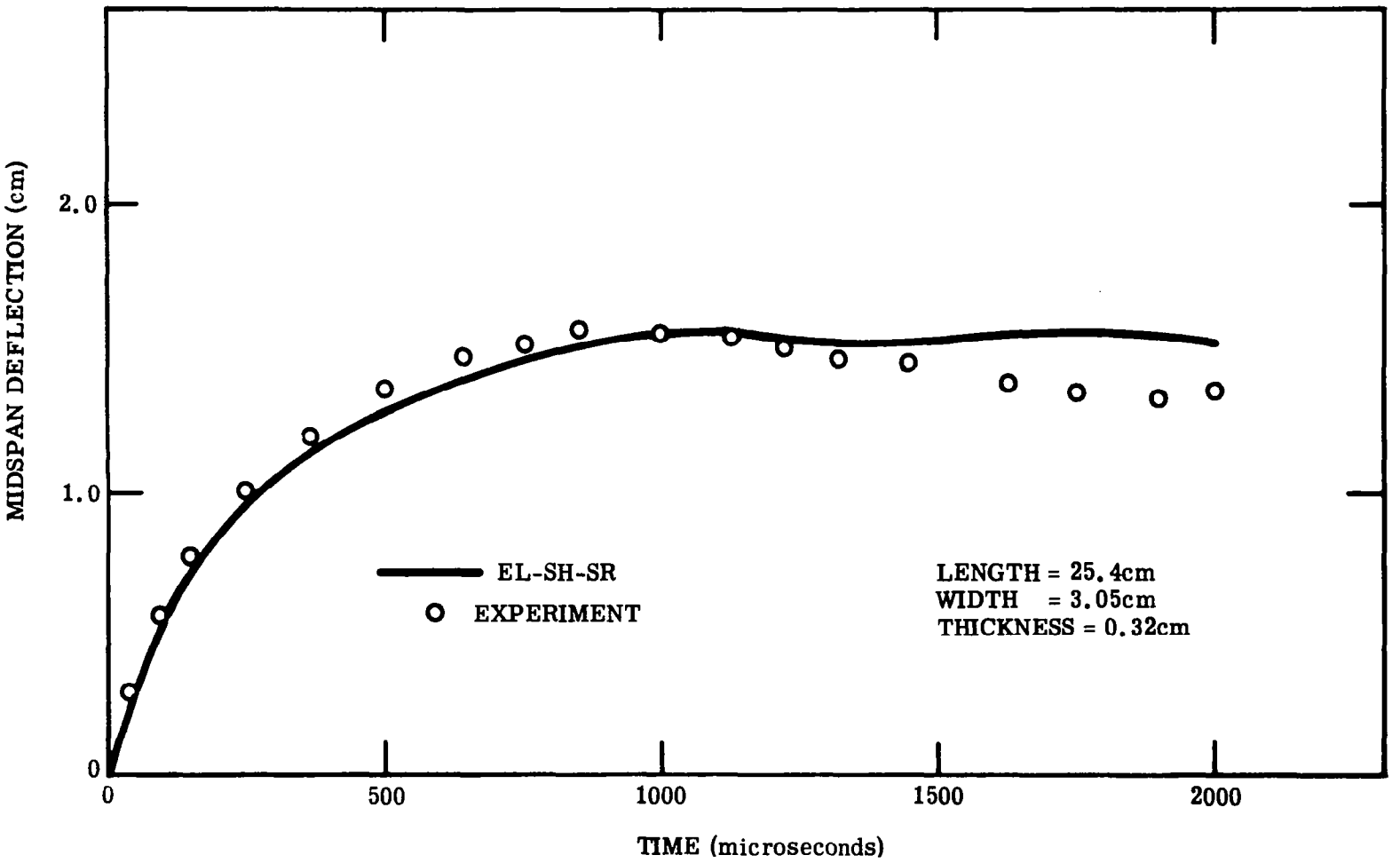

Fig. 12a Response of Explosively Loaded 1010 Steel Beam

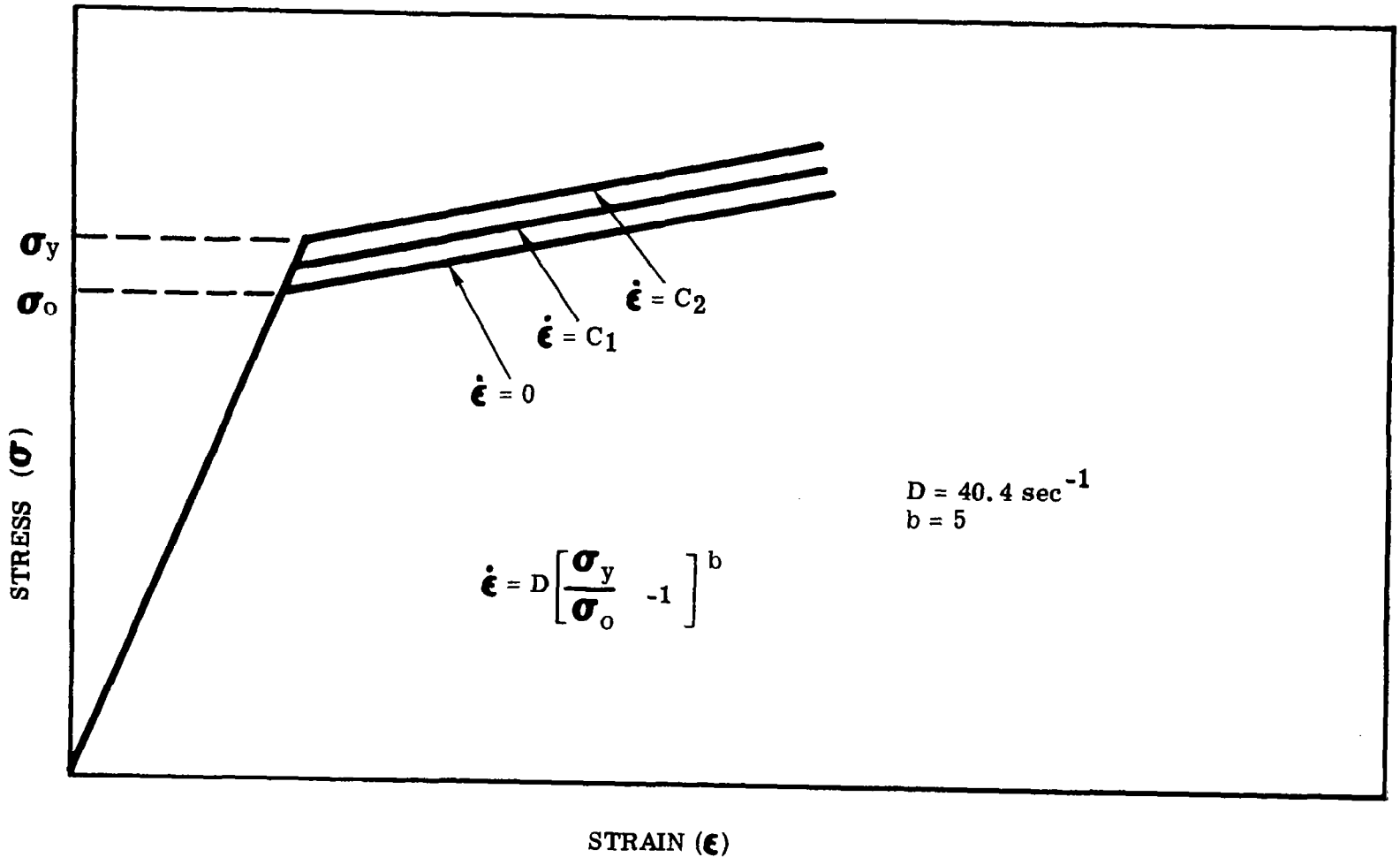

Fig. 12b Idealized Strain Rate Behavior for 1010 Steel

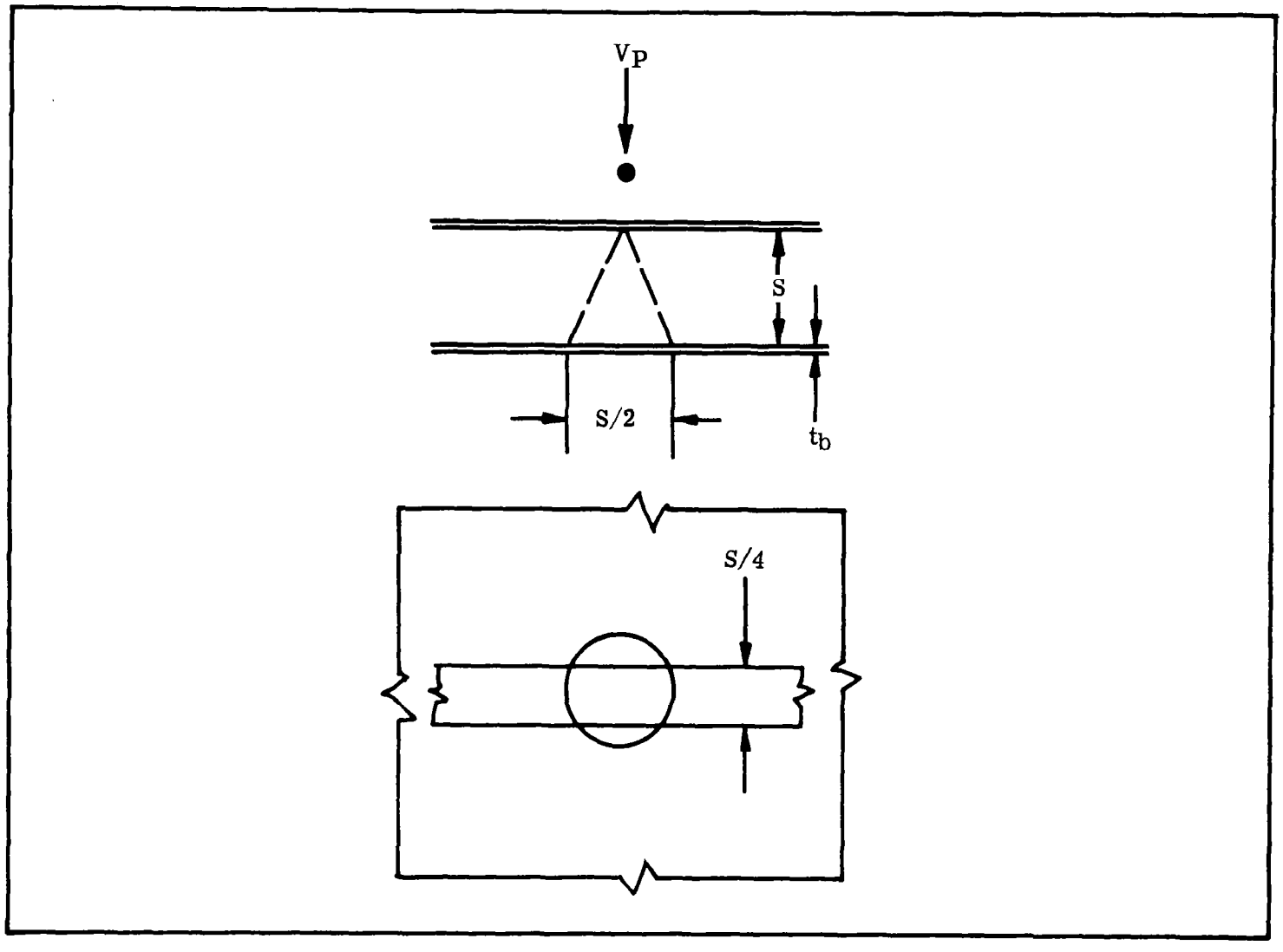

Fig. 13 Strip Approximation

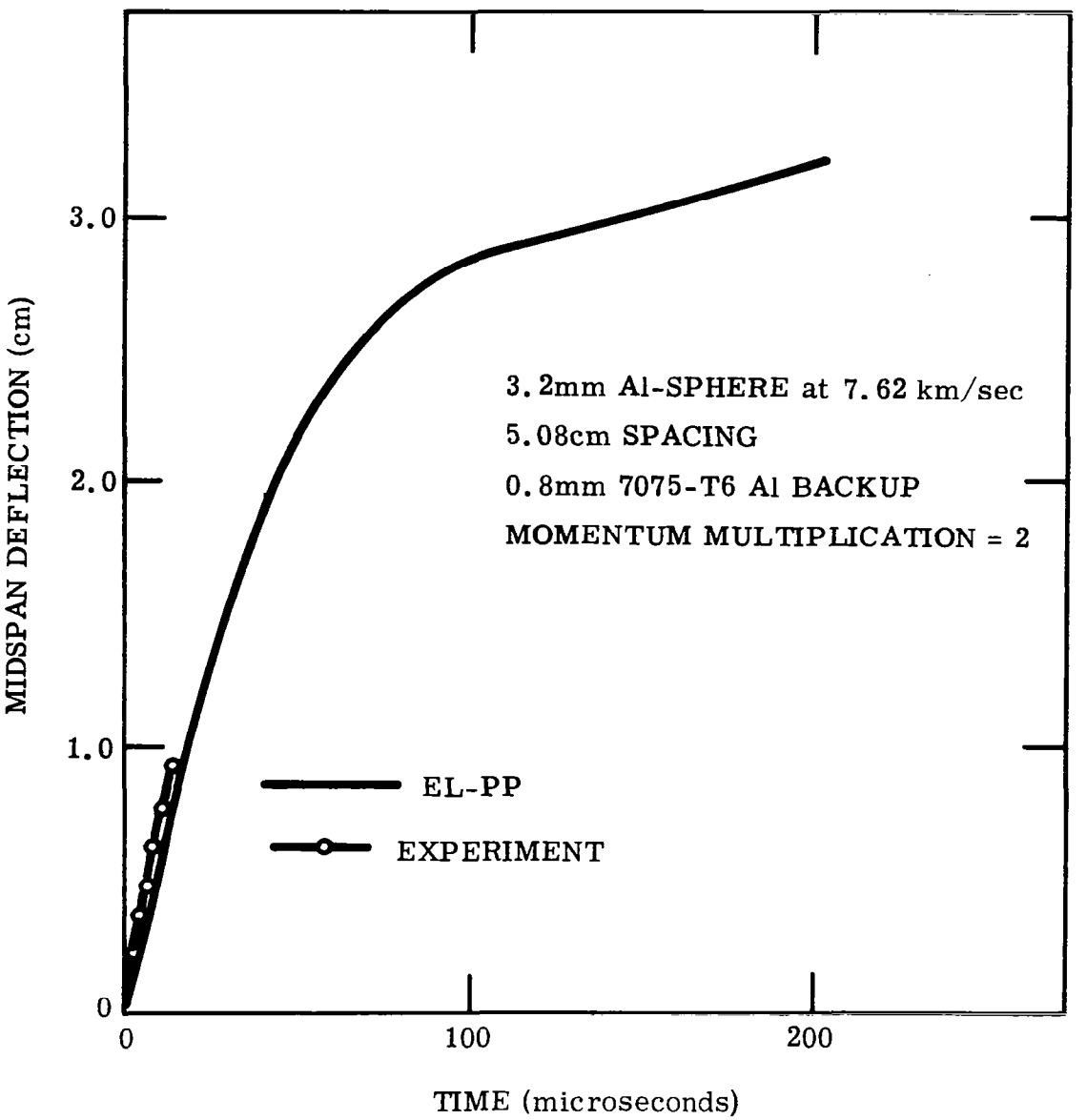

Fig. 14a Centerline Displacement vs Time for 3.2-mm Aluminum Sphere – 0.8-mm Backup

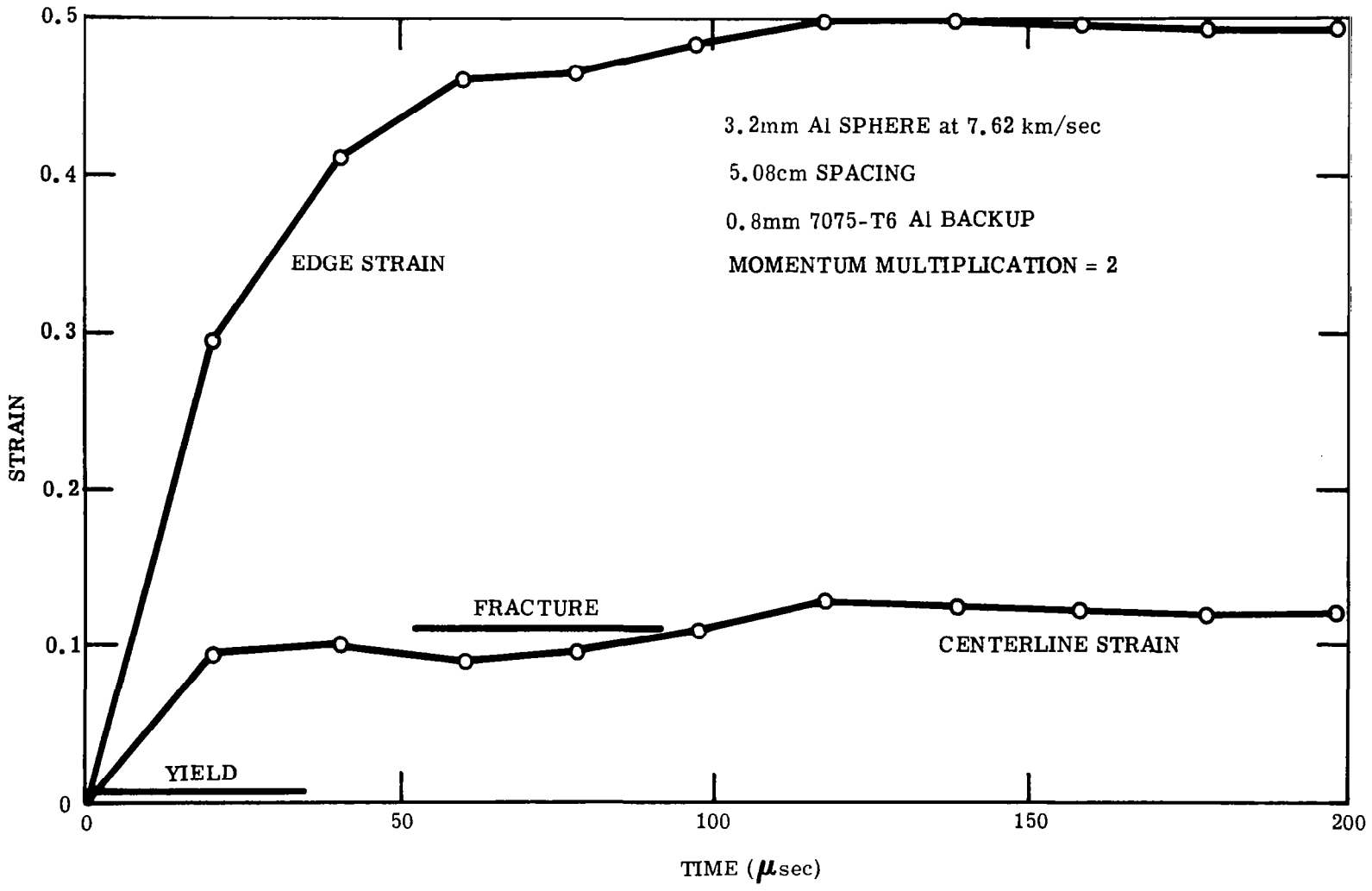

Fig. 14b Centerline and Edge Strain vs Time for 3.2-mm Aluminum Sphere – 0.8-mm Backup

theory and experiment. Note that in Fig. 14b the fracture strain is first reached at the edge of the loaded area after about 7 microseconds; after this time the solution is academic. Note also that there is some evidence of spalling in Fig. 10, and that such initial wave effects have been ignored for the moment.

The calculations were repeated for the above case, but with a backup sheet 1.6 mm thick. The results (Figs. 15a and 15b) show that now the peak strain occurs at the center of the sheet, and that the sheet should not fracture. Figure 9 shows that in practice only a small perforation occurs in the target, and this is due to spallation.

The Effect of Span

With the above reasonable agreement between theory and experiment, it was decided to use the strip approximation further. Also, because solutions are required for an effectively semi-infinite rear sheet, it was considered necessary to find out how long a strip is effectively semi-infinite for the time of interest in the present problem. To do this, the analysis of Fig. 14 (25.4-cm span) was repeated for a 50.8-cm span, with the result that up to about 100 microseconds no difference was found in centerline deflection, edge, or center strain for the two cases. Since in most situations of interest either the maximum or fracture strain would occur in less than 100 microseconds, it was decided that a 50.8-cm span would correspond to an effectively semi-infinite sheet and would be used in all subsequent calculations.

Complete Results for Particles with a Diameter of 3.2 mm

The strip approximation has been used to determine the response of backup sheets of various thicknesses for impacts of 3.2-mm particles at velocities of 7.62, 15.2, 22.8, and 30.4 km/sec. The results at 7.62 km/sec (Figs. 16a–16c) show that there is a large difference between backup sheet thicknesses required for no-yield (maximum strain less than 0.7%) and no-fracture (maximum strain less than 11%) failure. Also, it can be observed that for sheet thicknesses above about 1.6 mm the maximum strain occurs at the center of the plate, whereas for thinner sheets the maximum strain occurs at the edge of the loaded area. Similar solutions to Fig. 16 have been obtained for the other three impact

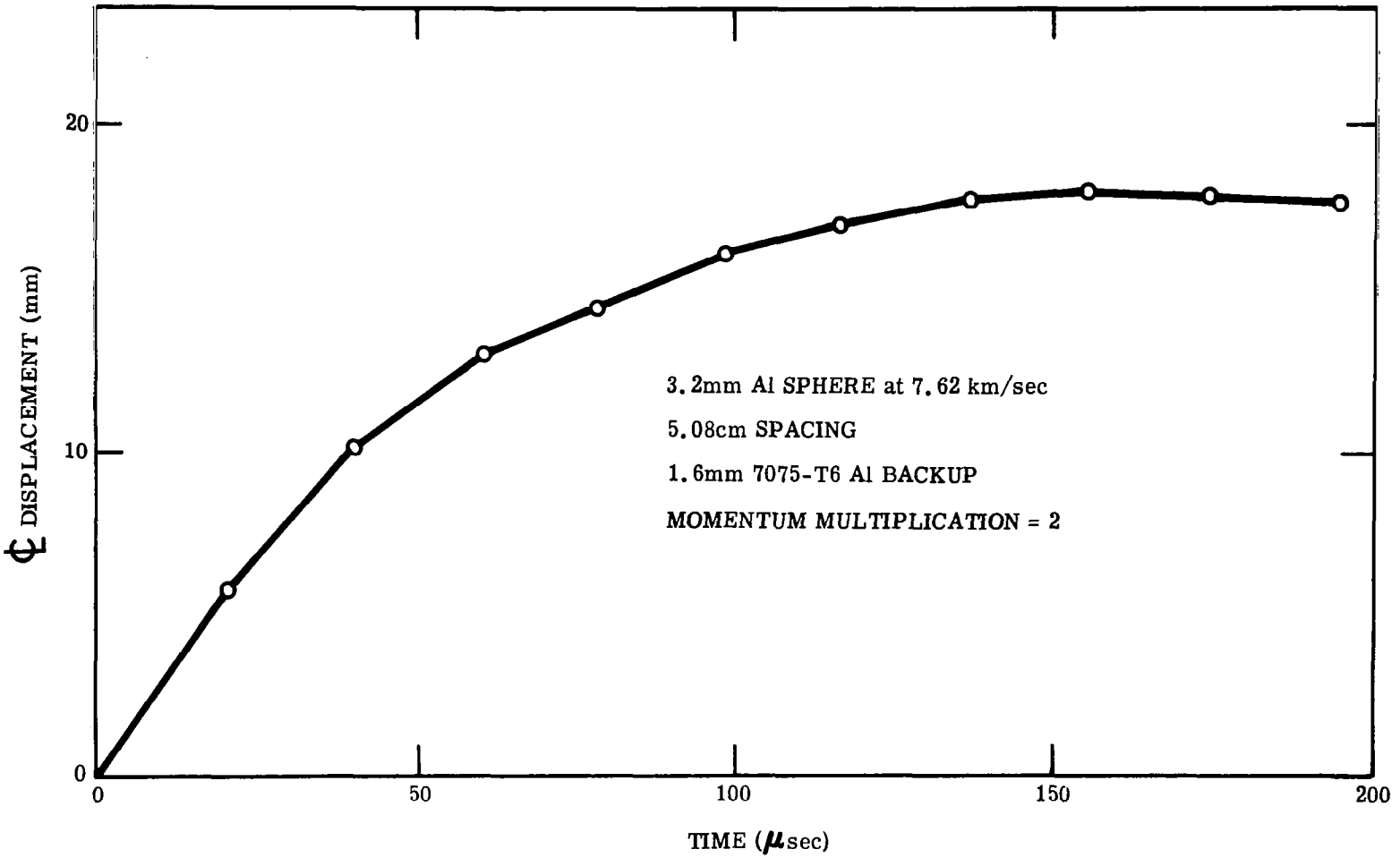

Fig. 15a Centerline Displacement vs Time for 3.2-mm Aluminum Sphere – 1.6-mm Backup

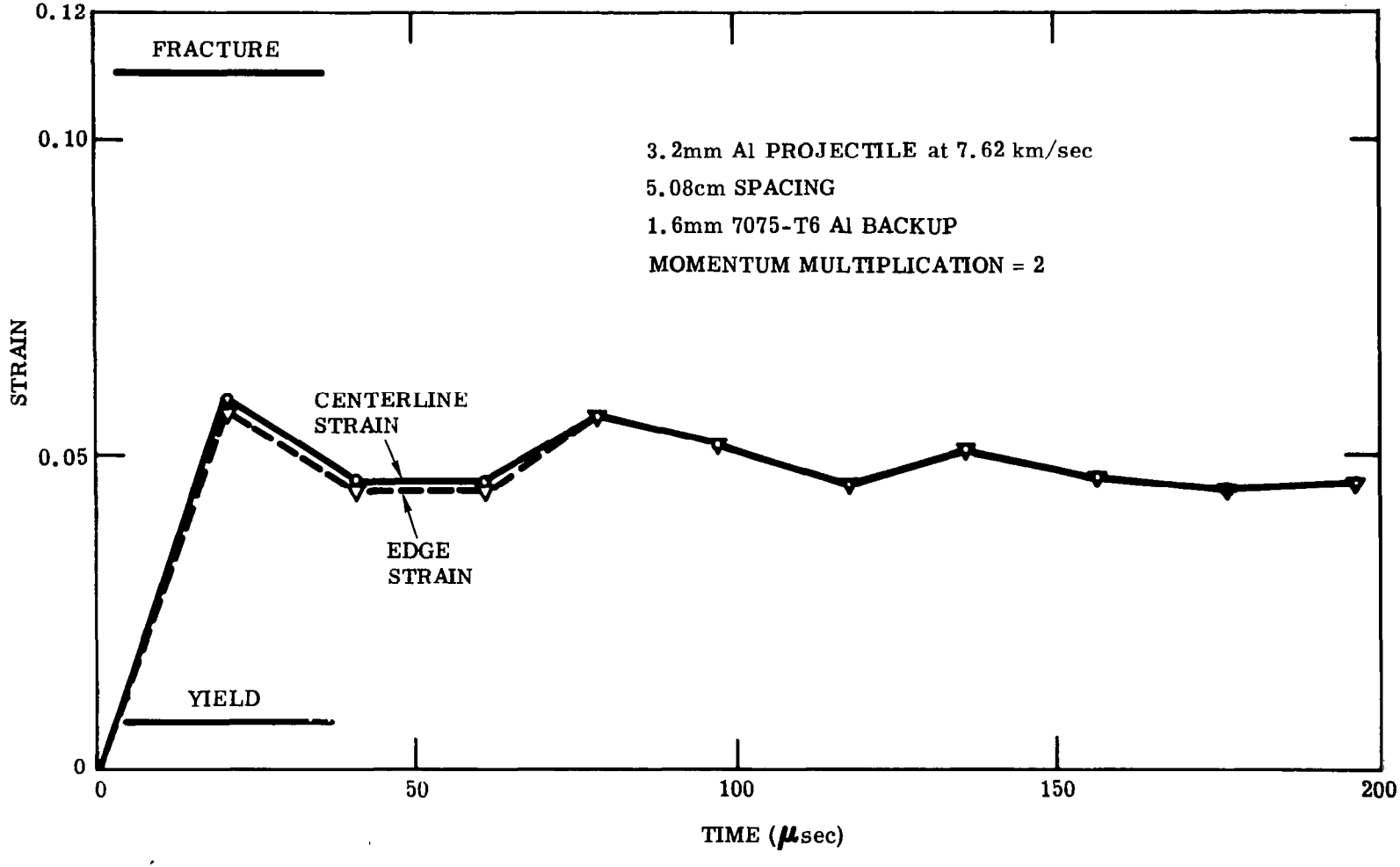

Fig. 15b Centerline and Edge Strain vs Time for 3.2-mm Aluminum Sphere – 1.6-mm Backup

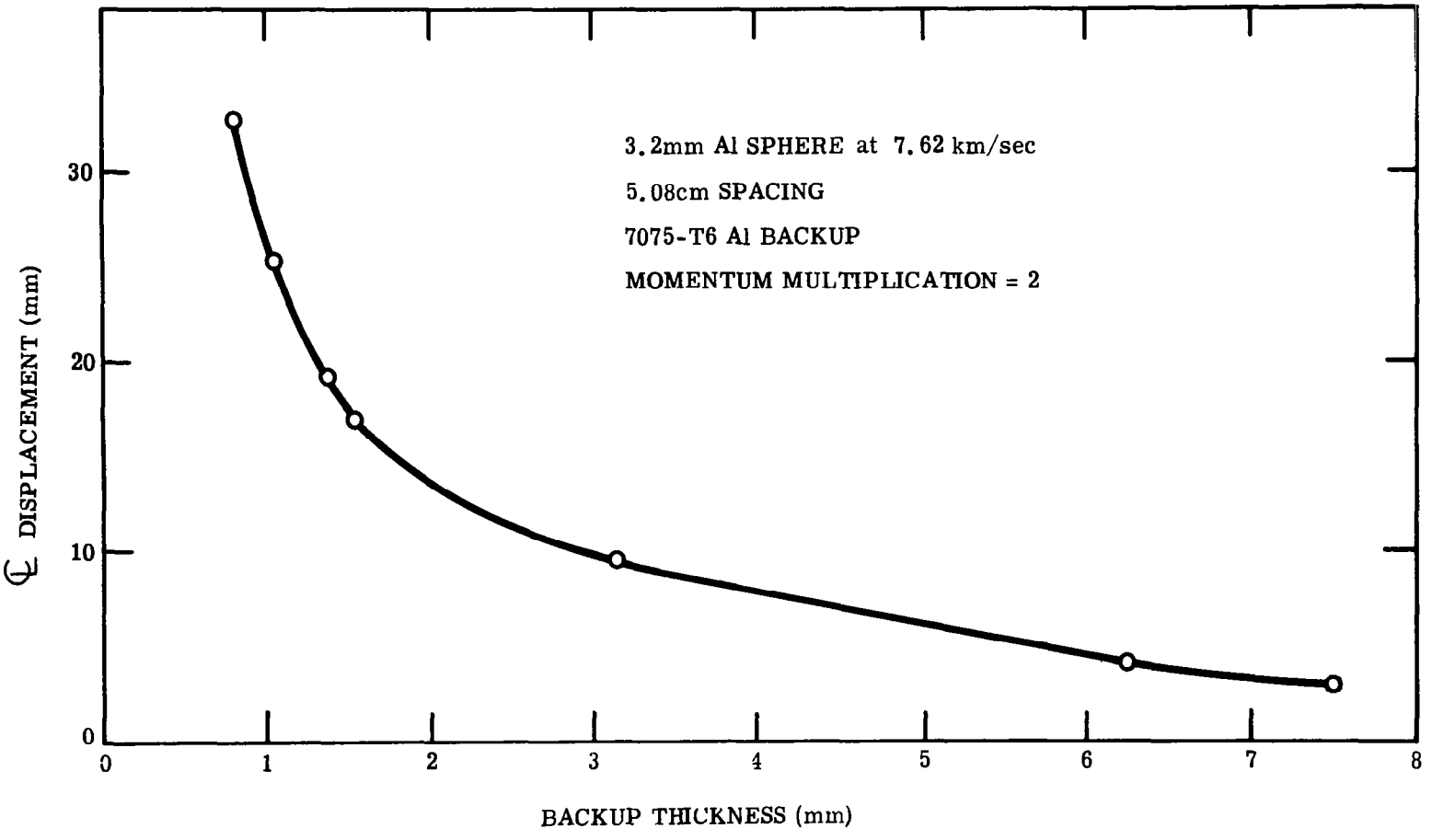

Fig. 16a Centerline Displacement vs Backup Thickness at 200 Microseconds for 3.2-mm Aluminum Sphere

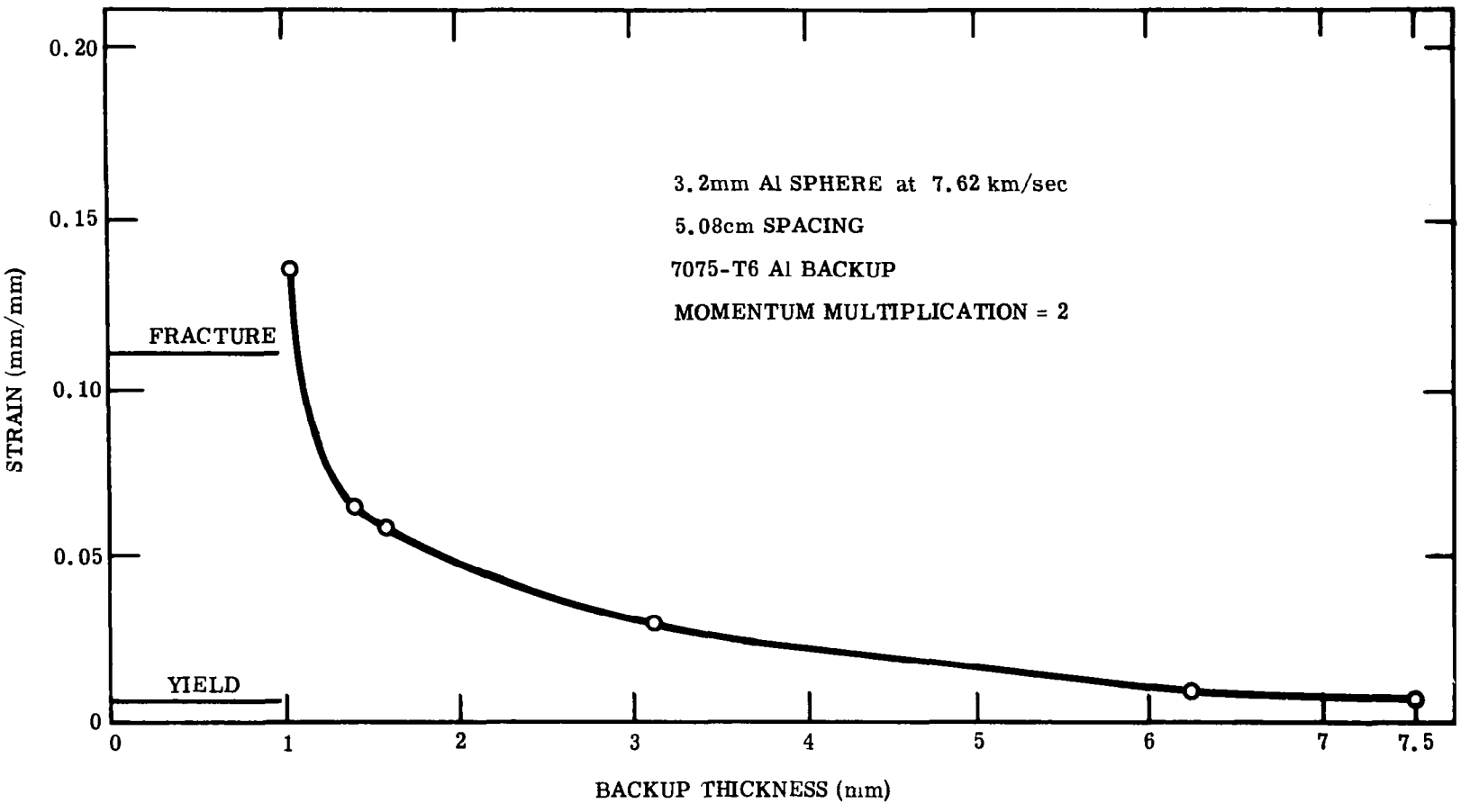

Fig. 16b Centerline Strain vs Thickness at 200 Microseconds for 3.2-mm Aluminum Sphere

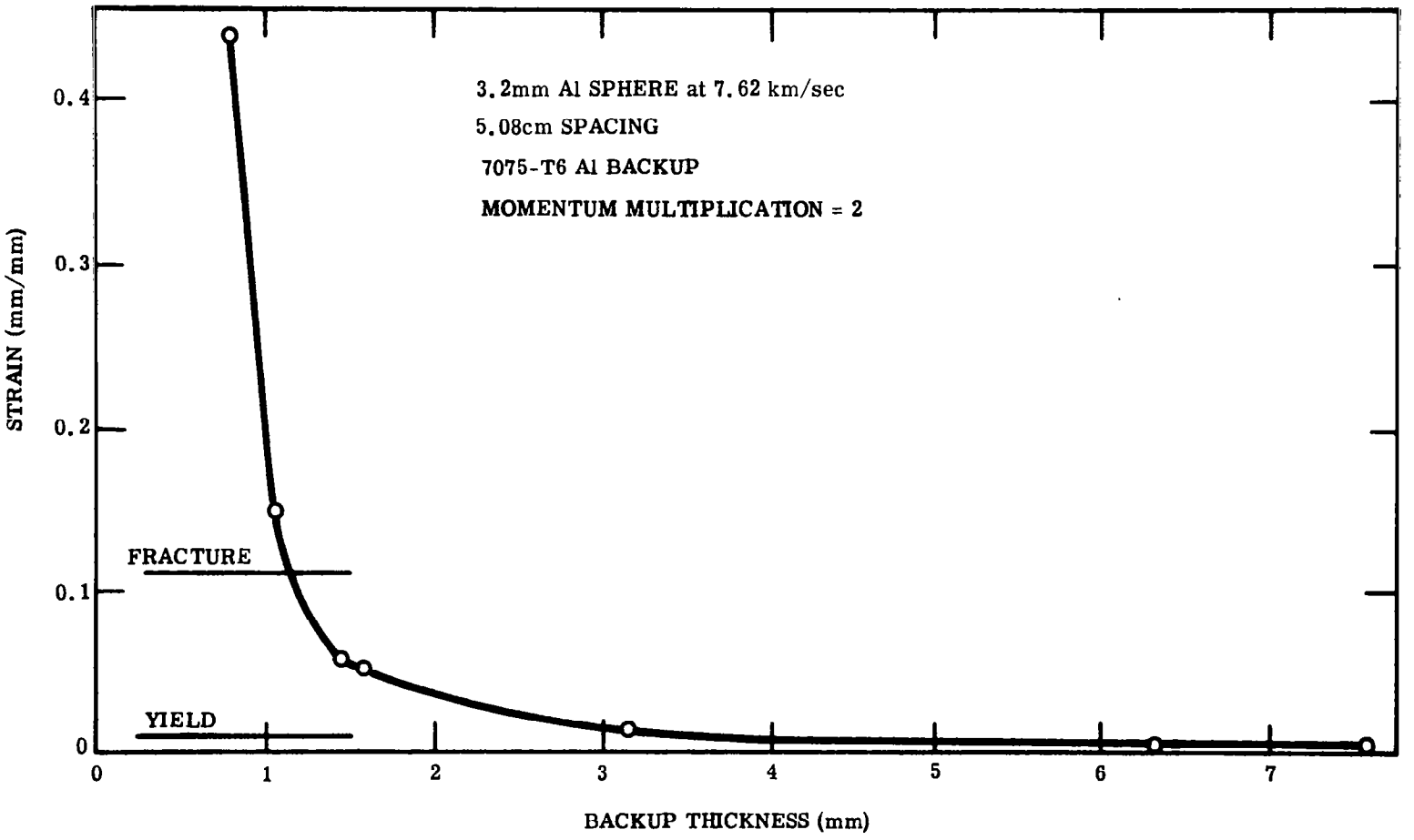

Fig. 16c Edge Strain vs Thickness at 200 Microseconds for 3.2-mm Aluminum Sphere

velocities. The resulting curves of sheet thickness against impact velocity for failure criteria of yield, maximum strain of 2%, 4%, and 6%, and fracture are presented in Fig. 17. The surprising aspect of this figure is that for each failure criterion the curve t_b against velocity is nearly linear. This is surprising in view of the fact that the basic mechanisms are nonlinear. It is also seen from the figure that above about 4% strain at a given velocity, a small change in thickness produces a large strain increment. Thus, it would appear wise to design for no more than a few percent maximum strain.

The Effect of Particle Size

Figures 18 and 19 show results similar to those of Fig. 17, but for 1.6-mm and 1.02-mm diameter aluminum spheres, respectively. The same comments can be made concerning the results for these particles that were made for the 3.2-mm particle. Note that the crowding of the constant maximum strain lines is seen to increase with decreasing particle size.

From the above figures, the backup sheet thicknesses for the yield and fracture criteria have been plotted against particle diameter at 7.62, 15.2, 22.8, and 30.4 km/sec. Inspecting the results (Figs. 20 and 21) reveals that for either criterion, and at a constant impact velocity, t_b is approximately proportional to the cube of the particle diameter. Thus, under these conditions, Eq. (2) indicates that v_i, the initial velocity of the loaded area, is essentially constant. Another way of looking at this is to say that with particles of various sizes an approximately constant maximum strain will be obtained, provided that the applied momentum per unit sheet thickness is held constant.

The Effect of Spacing

Spacings of 2.54, 5.08, and 10.16 cm were investigated for the Apollo particle (1.02-mm diameter) at 30.4 km/sec. The results for both the yield and fracture criteria (Fig. 22) show that the sheet thickness necessary for either decreases approximately with the inverse square of spacing. This result, plus those of the preceding sections, gives rise to an approximate equation for rear sheet thickness. For 7075-T6 aluminum this equation is given by

$$t_b = C \frac{M_p V_p}{S^2} \qquad (3)$$

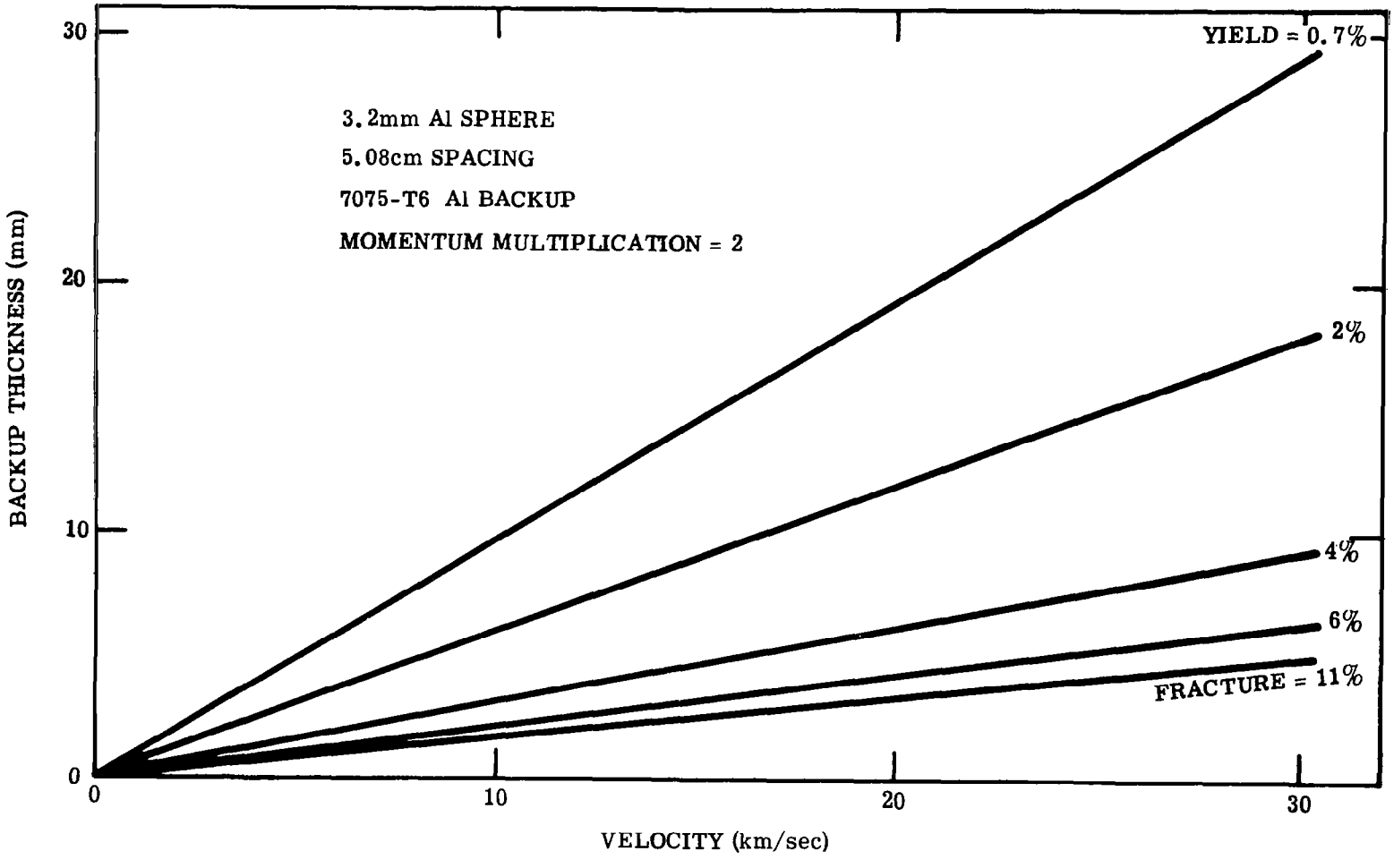

Fig. 17 Backup Thickness vs Velocity for 3.2-mm Aluminum Sphere

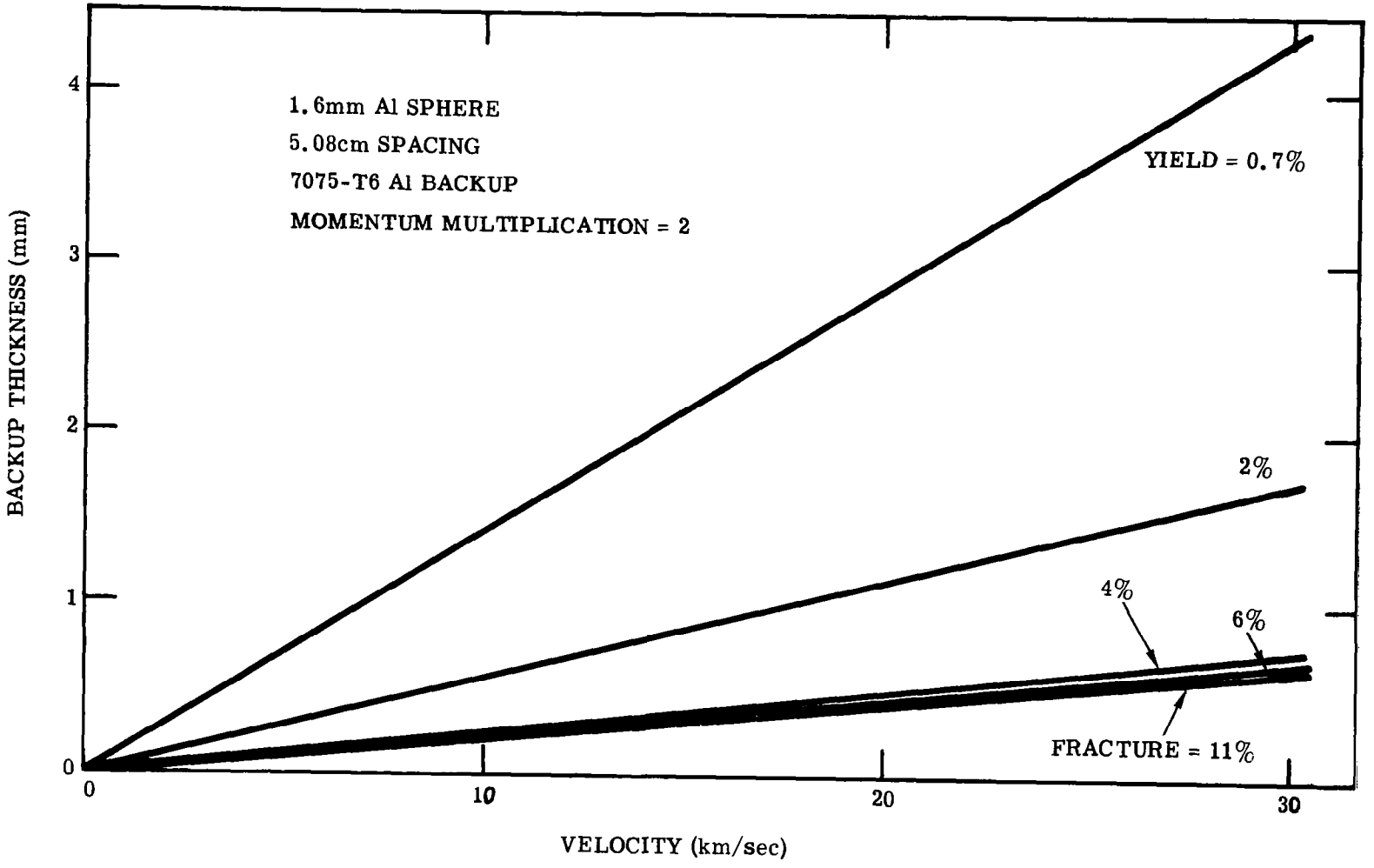

Fig. 18 Backup Thickness vs Velocity for 1.6-mm Aluminum Sphere

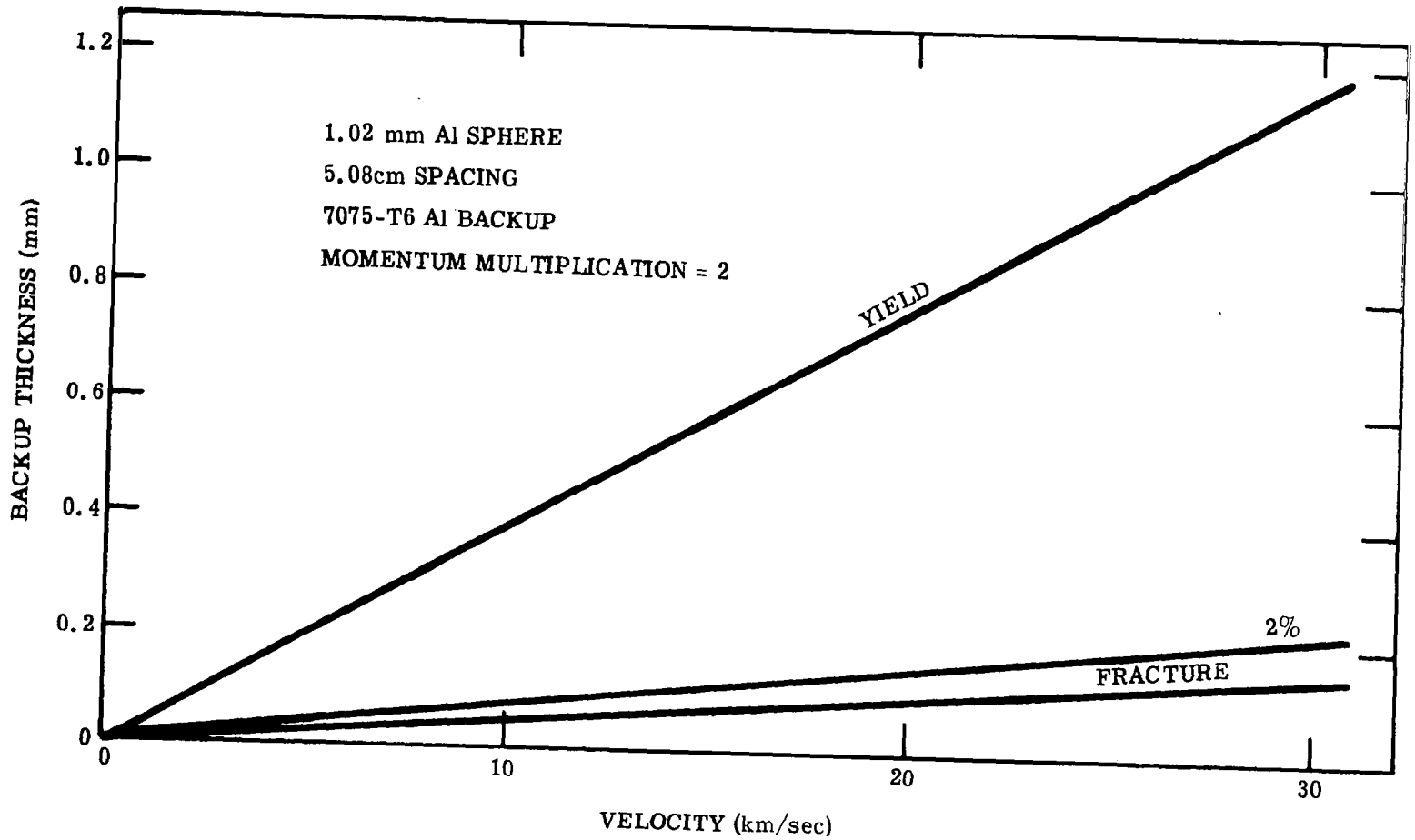

Fig. 19 Backup Thickness vs Velocity for 1.02-mm Aluminum Sphere

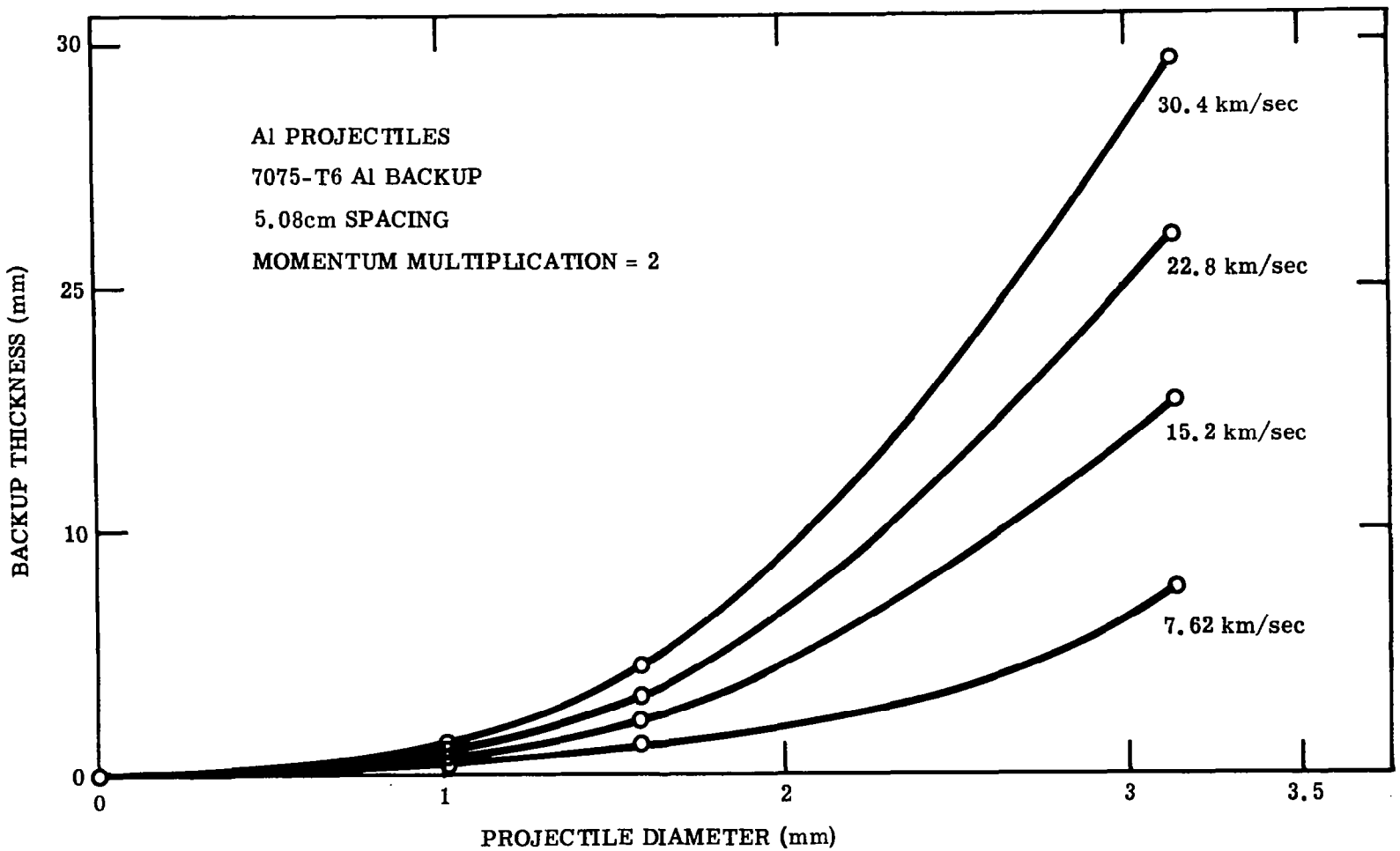

Fig. 20 Backup Thickness vs Particle Diameter to Prevent Yield

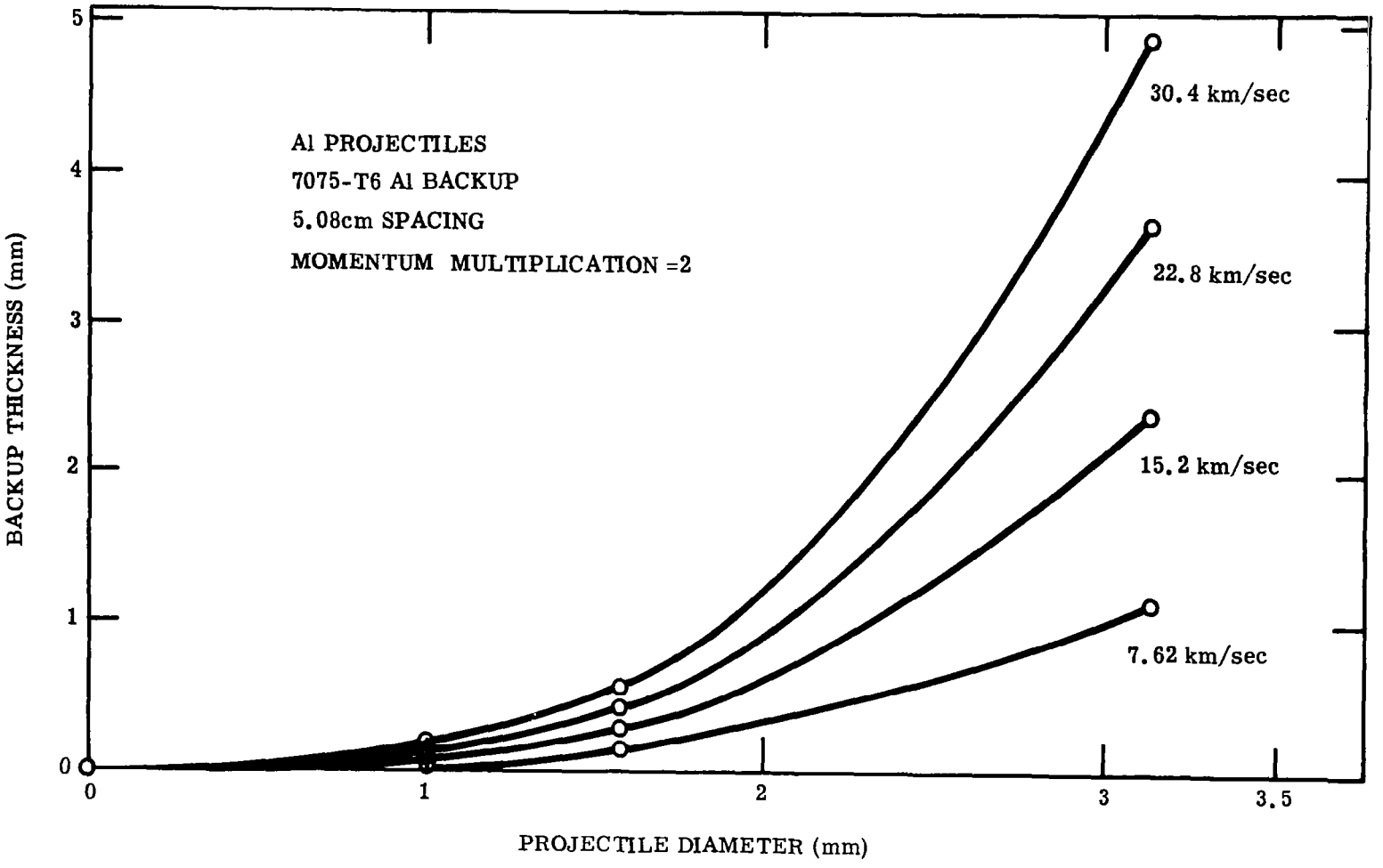

Fig. 21 Backup Thickness vs Particle Diameter to Prevent Fracture

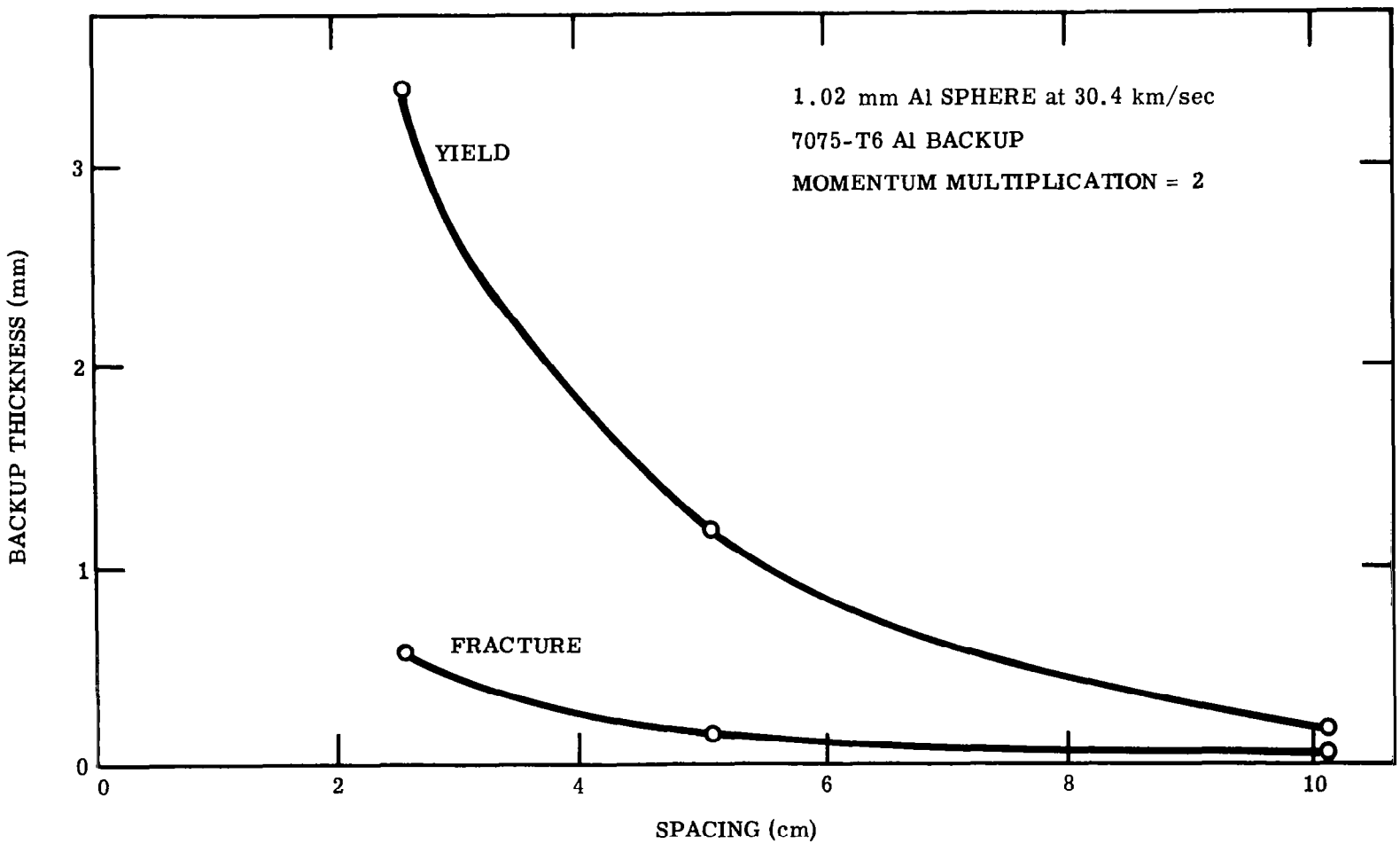

Fig. 22 Backup Thickness vs Spacing for 1.02-mm Aluminum Sphere Impacting at 30.4 km/sec

where $C = 415 \pm 140$ and 82 ± 14 for the yield and fracture criteria, respectively, t_p is in millimeters, M_p is in grams, V_p is in km/sec, and S is in centimeters. Note: because the exact solutions do not require v_i in Eq. (2) to be exactly constant, there is not a constant value for C at a specific maximum strain.

The Effect of Pre-Tensioning the Backup Sheet

In many space applications the structure to be protected will be a pressurized fuel tank; hence, it was decided to investigate the effect of pre-tensioning the rear sheet (in one direction only). Since the computer code for the strip approximation can accommodate such pre-tensioning, solutions were obtained for a 1.02-mm particle at 30.4 km/sec with pre-tensioning of 25%, 50%, 75%, and 100% static yield stress. The centerline displacements against time are shown in Fig. 23, which gives evidence that pre-tensioning can significantly decrease the deflection of the sheet. Also, the sheet thicknesses required for both the yield and fracture criteria are shown in Fig. 24. These results reveal that the thickness required for the yield criterion is not very sensitive to pre-tension, whereas the thickness based on the fracture criterion is sensitive to the amount of pre-tension.

Extensions of the Strip Approximation

The strip approximation has been shown to be in remarkably good agreement with experimental results; however, the complete solution should consider a centrally loaded circular plate. The numerical technique of Witmer, et al.,[10] has been applied to the plate analysis and is being checked out on the 7040 computer at GM Defense Research Laboratories. Hopefully, the results of this analysis can soon be compared with those from the strip approximation.

Note that either strip approximation or complete plate analysis can be used to analyze impacts in multisheet targets by summing the momentum in the loaded segment of a sheet at the time fracture occurs around the circumference of the loaded area. This gives the momentum (reduced from twice the original particle momentum) to be applied to the next sheet in the array. The analysis is then continued until either a sheet is not perforated or the last sheet is reached.

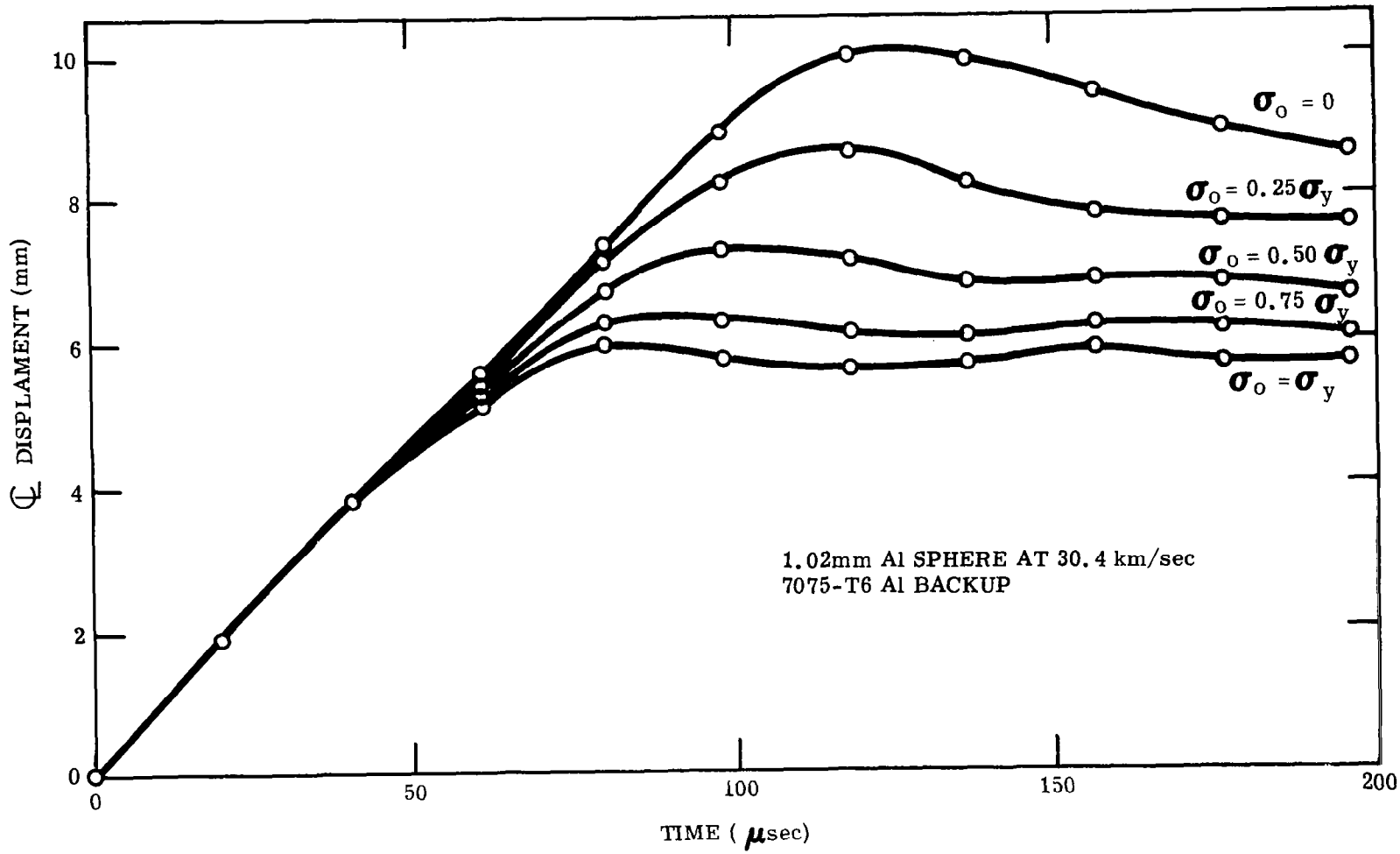

Fig. 23 Centerline Displacement vs Time – Pre-Tensioned Beam

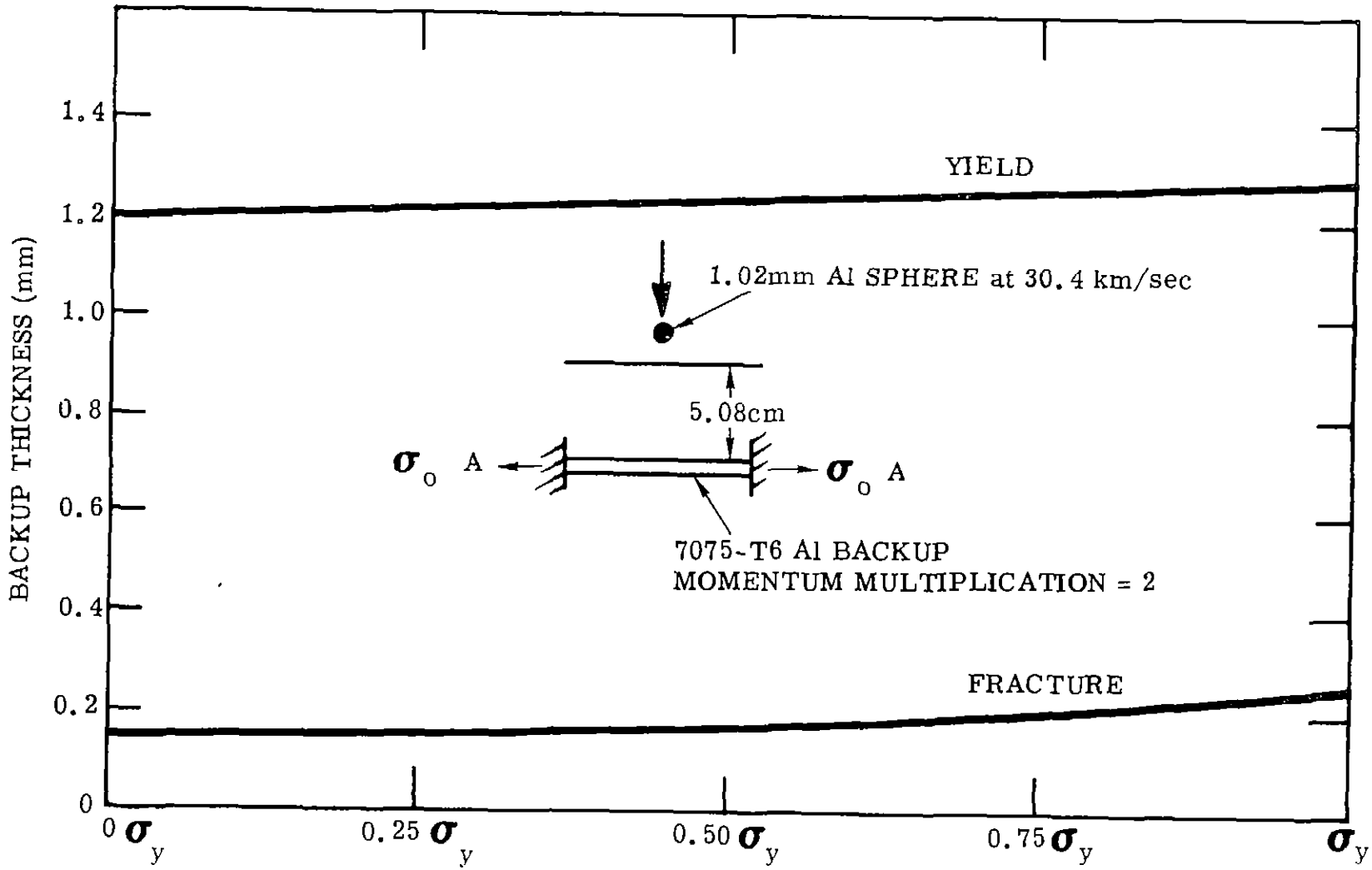

Fig. 24 Backup Thickness vs Pre-Tension Stress

INTERACTION OF DEBRIS WITH A SHIELDED TARGET – EXPERIMENTAL

Momentum Multiplication

Experiments using a "ballistic pendulum" to measure the momentum imparted to a shielded structure have started, with 3.2-mm aluminum projectiles, spacing of 5.08 cm, and shields of 1100-0 aluminum (t_s/d = 0.1, 0.2, 0.3, and 0.5). The results are presented in Figs. 25 and 26. Figure 25 shows that with a constant value of t_s/d, the momentum multiplication factor does not increase very rapidly with increasing impact velocity; and when t_s/d = 0.2 (near optimum) the factor rises only to a value of about 1.3. That a momentum multiplication factor of two was not obtained in these tests is no surprise, for at these velocities the debris impacting the pendulum will not be gaseous.

Figure 26 shows, as a function of shield thickness, the momentum multiplication factor at velocities of 4.8 and 7.6 km/sec. It is seen that the optimum shield thickness is fairly insensitive to velocity. Also, the optimum shield thickness at 7.6 km/sec agrees well with the theoretical optimum in Fig. 7.

Several other isolated ballistic pendulum tests have been conducted. For instance, two 3.2-mm aluminum projectiles were fired at 6.46 km/sec against 1100-0 aluminum shields, 1.02 mm thick and spaced at 1.27 cm and 5.08 cm from the pendulum. In both cases, the momentum multiplication factor was found to be about 1.3 and thus essentially independent of spacing.

Finally, a few tests were made with cadmium shields and projectiles. Projectiles were 3.2 mm in diameter and spacing was 5.08 cm in all cases. Shield thicknesses were such that t_s/d equaled 0.1 and 0.2. The advantage of conducting such tests can be seen in Fig. 8 which shows that, over the experimental range of velocities, all possible states of debris can be produced in the bubble. The object was to find out whether a momentum multiplication factor of two would be produced when a large proportion of the debris in the bubble was in the gaseous state.

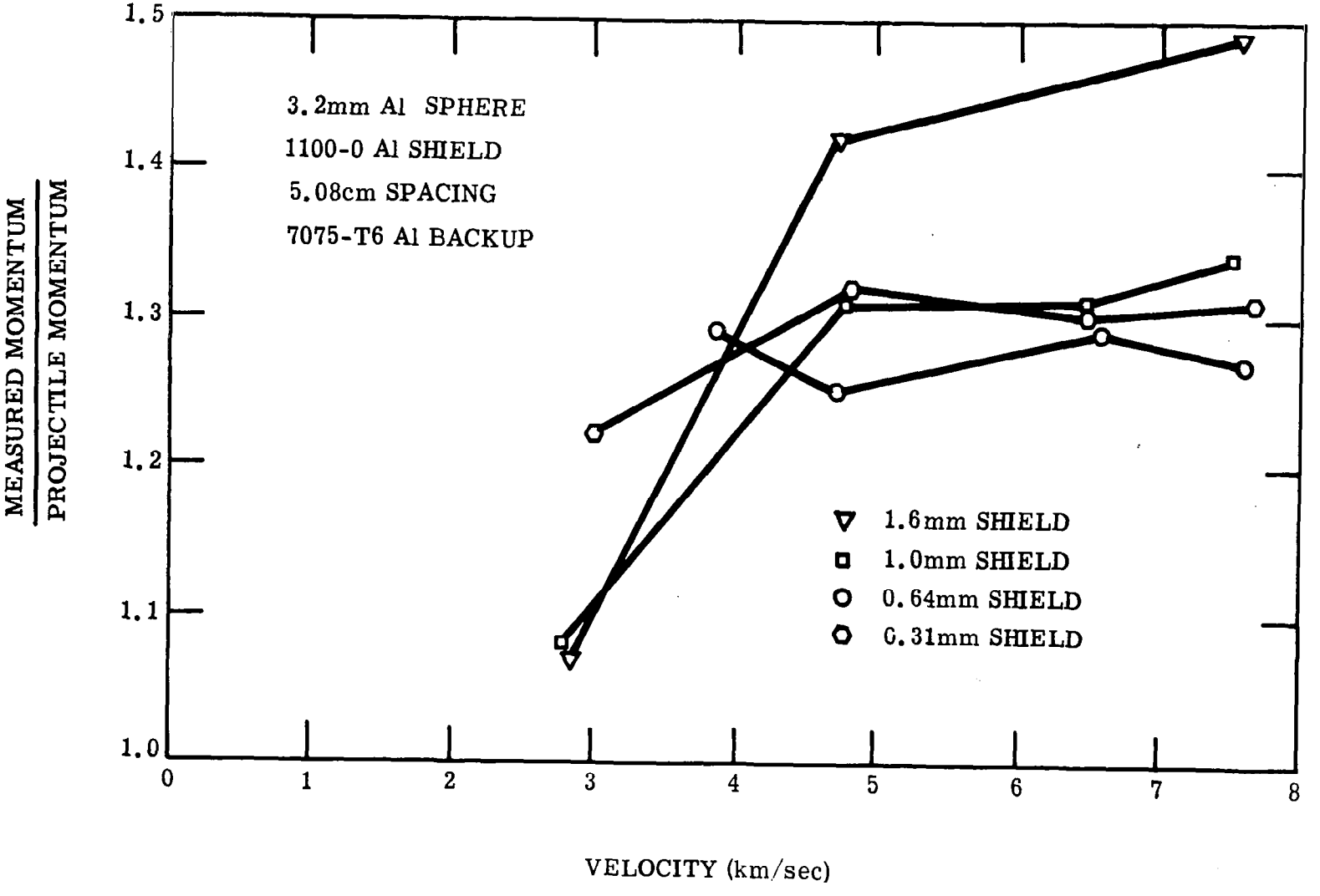

Fig. 25 Momentum Multiplication vs Velocity

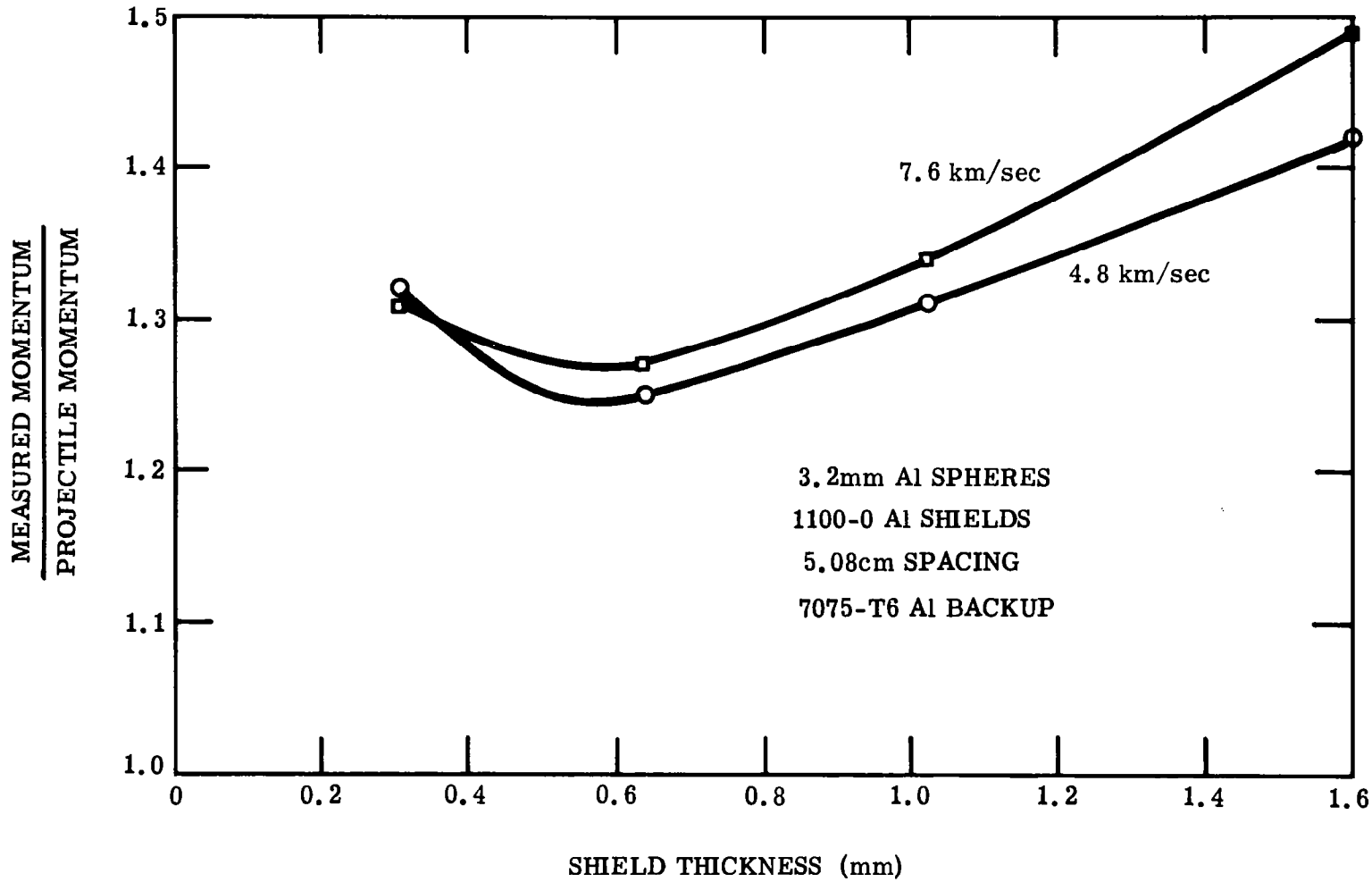

Fig. 26 Momentum Multiplication vs Shield Thickness

The results of the tests show that when $t_s/d = 0.2$, momentum multiplication factors of 1.16 and 1.41 were obtained at velocities of 3.5 and 6.5 km/sec, respectively. At 6.5 km/sec the debris is expected to contain large amounts of gas; hence, obtaining a value as low as 1.41 for the momentum multiplication factor is at first surprising. However, two points should be made. The first is that a comparison of these two values for $t_s/d = 0.2$ with those for $t_s/d = 0.2$ in Fig. 25 shows that the presence of gas in the debris significantly increases the momentum multiplication factor. The second point is that the momentum multiplication factor is seen to increase quite rapidly as the velocity, and hence the proportion of gas in the debris, increases. Consequently, as the impact velocity increases, the momentum multiplication factor may approach a value of two. Only one experiment has been conducted at $t_s/d = 0.1$, when a momentum multiplication factor of 1.34 was obtained at 5.6 km/sec. This value of 1.34 is also higher than the comparable value for aluminum from Fig. 25.

Experimental Check of Predictions for a 1.02-mm Aluminum Particle at 30.4 km/sec

Several experiments were conducted to check the validity of the calculation shown in Fig. 19 for a particle with a diameter of 1.02 mm (Apollo) at 30.4 km/sec. The momentum of this particle at 30.4 km/sec is nearly the same as a particle with a diameter of 1.6 mm at 7.8 km/sec. Assuming the momentum multiplication factor to be the same at both velocities, a 0.6-mm-diameter particle at 7.8 km/sec can simulate the backup sheet loading from the Apollo particle at 30.4 km/sec. For this reason tests have been conducted with 1.6-mm aluminum particles at 7.8 km/sec, spacing of 5.08 cm, 0.31-mm shields of 1100-0 aluminum (near optimum), and 7075-T6 aluminum backup sheets, 0.41, 0.82, and 1.64 mm thick. Photographs of the two thinnest backup sheets (Fig. 27) show that neither failed due to impact. This is consistent with the results of Fig. 19, where it is predicted that a 1.02-mm aluminum projectile should not fracture such sheets at 30.4 km/sec. Also consistent with the predictions of Fig. 19 is the lack of any deformation of the 1.64-mm backup sheet (not shown in Fig. 27).

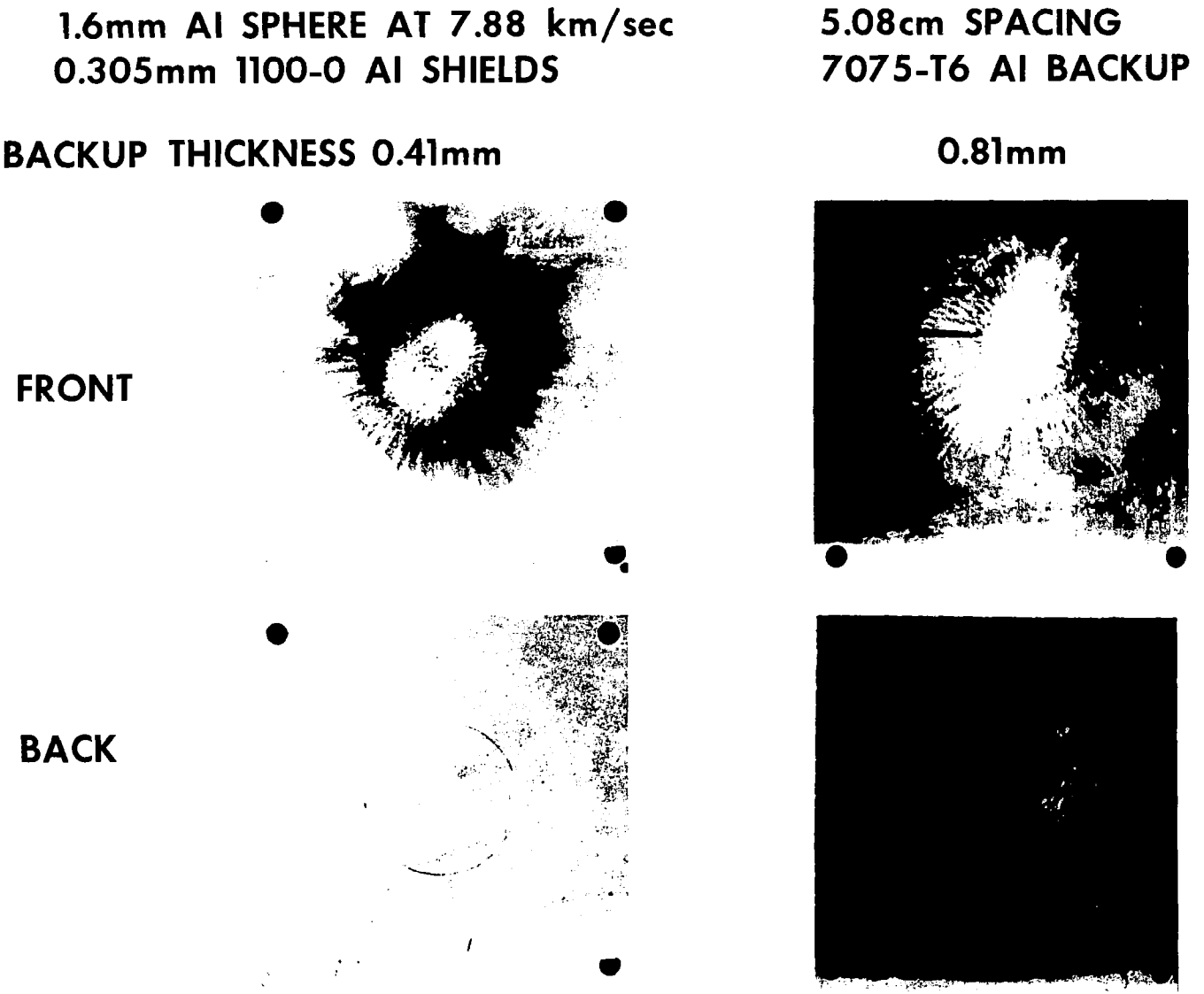

Figure 27 Backup Targets – Simulated Apollo Impacts

Spalling Experiments

As mentioned earlier in this paper, spalling, as well as gross deformation of the rear sheet, is a possible damage mechanism. However, it is interesting to observe that no spallation occurred in the very thin targets shown in Fig. 27. The reason for this was revealed by repeating the above experiments with very thin 7075-T6 pellets (6.35 mm in diameter and 0.41 mm thick) lightly glued to the rear surface of the backup sheets. Upon impact, the pellets trapped some of the momentum in the spall-producing wave, and their resultant velocities were measured with the B&W framing camera. The fastest pellet from each impact was then considered, and it was assumed that the particle velocity v behind the wave in the target was equal to half the measured pellet velocity v_p. The stress in the wave reaching the rear surface of the target is thus given by

$$\sigma = \rho c v = \rho c v_p/2$$

where c and ρ are the dilatational wave velocity and density of the target material. The value of σ for the 0.41-mm backup sheet was found to be 5.95 kilobars, and for the 1.64-mm sheet, 1.88 kilobars. These values are much less than the value of approximately 14 kilobars necessary to spall 7075-T6 aluminum; hence, the absence of spalling in the targets shown in Fig. 27 is no surprise.

Two additional pellet tests were conducted using cadmium projectiles and shields. In the first test, the projectile was a 3.2-mm cadmium sphere at 6.46 km/sec, the spacing was 5.08 cm, and the cadmium shield was 0.64 mm thick. In the second test, the projectile was a 4-mm cadmium sphere at 3.44 km/sec, the spacing was 5.08 cm, and the cadmium shield was 0.76 mm thick. These tests were chosen so that the momentum felt by a backup target would be approximately the same at each set of test conditions. Measurements with the ballistic pendulum showed that this was approximately so (actually, the momentum felt by the backup sheet at the higher velocity turned out to be 1.13 times that at the lower velocity). Thus, the total impulse applied to a target was approximately the same for the two sets of conditions, with the object of finding out whether the pressure pulse became more or less effective in producing spallation as the impact velocity increased. This point was considered important in assessing

the 30.4 km/sec simulated Apollo particle tests described in the previous section because, even though the gross deformation characteristics at 30.4 km/sec can be simulated at lower velocities, it is not at all evident that this simulation holds for the spalling effects. Hence the results of the cadmium tests prove very interesting.

The backsheets were plates of 7075-T6 aluminum. No spall formed at the higher velocity, whereas a spall formed at the lower velocity. These observations are consistent with the pellet results, which showed a stress of 22 kilobars at the lower velocity and 7.7 kilobars at the higher velocity.

DISCUSSION AND CONCLUSIONS

The large dynamic deformation analysis used to predict backup sheet thicknesses has been found to give results that are in reasonable agreement with experimental results. Even better agreement is expected when the plate analysis, rather than the strip approximation, is used. Further experiments will be necessary to accurately define the momentum multiplication factor and distribution of loading applied to the backup sheet. Indications are that a momentum multiplication of two is too high, even at 30 km/sec. In this regard, note that the same agreement between theory and experiment in Fig. 15a can be obtained if a momentum multiplication of 1.27 (from Fig. 26) and a load spread uniformly over a circle 3/8 S in diameter (from Fig. 10) is used in the analysis. Further experiments are planned to define these load parameters more exactly; and additional work is to be conducted on spalling, even though present indications are that the backup sheet thickness, determined by the gross deformation analysis with a no-yield failure criterion, is thick enough not to spall.

The interest in Project Apollo makes it pertinent to summarize the conclusions regarding shielding requirements for this mission. The critical meteoroid mass was shown earlier to be the same as that of a 1.02-mm-diameter aluminum sphere, and Fig. 7 shows that for this particular particle a 0.20-mm aluminum shield ($t_S/d = 0.19$) will be adequate at velocities above 7 km/sec. Figure 19 shows also that, for a spacing of 5.08 cm and a velocity of not more than 30 km/sec, a 1.20-mm-thick backup sheet of 7075-T6 aluminum will not yield. Thus, the total thickness of the structure, 1.40 mm, must now be assessed to determine if it will resist penetration at velocities below 7 km/sec.

From Fig. 5 it is estimated that, for $t_S/d = 0.19$, the maximum value of normalized penetration (p_T/d) is 0.9. Consequently, for a 1.02-mm aluminum particle, the maximum depth of penetration is 0.92 mm, occurring at about 3 km/sec. Since this value of p_T is for an effectively semi-infinite backup sheet of 2024-T3 aluminum, a correction factor must be applied for the finite thickness of the backup sheet and the different aluminum alloy. Preliminary experiments indicate that the backup sheet thickness must be boosted to about 1.40 mm to prevent penetration and spalling,

increasing the necessary thickness of the total structure to 1.60 mm. Interestingly, for this particular mission the greatest hazard is from low velocity meteoroids. Note that although only the simplest spacecraft structure has been considered in the example above, the techniques described in the body of this report can readily be extended to other combinations of impact conditions, materials, and spacings.

REFERENCES

1. C.J. Maiden, "Experimental and Theoretical Results Concerning the Protective Ability of a Thin Shield Against Hypervelocity Projectiles," Proc. of Sixth Hypervelocity Impact Symposium, 1963

2. C.J. Maiden, "Meteoroid Impact," Space Exploration, John Wiley and Sons, 1964

3. F.L. Whipple and R.F. Hughes, "On the Velocities and Orbits of Meteors, Fireballs, and Meteorites," Meteors, Pergamon Press Ltd., 1955, pp. 149–156

4. F.L. Whipple, "On Meteoroids and Penetration " (paper presented to the Interplanetary Missions Conference of the American Astronautical Society, January, 1963)

5. E.J. Opik, "Problems in the Physics of Meteors," Am. J. Phys., Vol. 26, No. 2, 1958

6. "Meteoroid Environment in Near Earth, Cislunar, and Near Lunar Space," NASA MSC Engineering Criteria Bulletin EC-1, 1963

7. A.E. Olshaker and R.L. Bjork, "Hydrodynamics Applied to Hypervelocity Impact, II The Role of Melting and Vaporization in Hypervelocity Impact," Proc. of Fifth Hypervelocity Impact Symposium, Denver, Colorado, 1961

8. R.G. McQueen and S.P. March, "Equations of State for Nineteen Metallic Elements from Shock Wave Measurements to Two Megabars," J. Appl. Phys., Vol. 31, No. 7, 1960

9. G.R. Fowles, "Attenuations of the Shock Wave Produced in a Solid by a Flying Plate," J. Appl. Phys., Vol. 31, 1960

10. E.A. Witmer, H.A. Balmer, J.W. Leech, and T.H.H. Pian, "Large Dynamic Deformation of Beams, Rings, Plates, and Shells," AIAA J., Vol. 1, No. 8, 1963, p. 1848

"The aeronautical and space activities of the United States shall be conducted so as to contribute . . . to the expansion of human knowledge of phenomena in the atmosphere and space. The Administration shall provide for the widest practicable and appropriate dissemination of information concerning its activities and the results thereof."

—NATIONAL AERONAUTICS AND SPACE ACT OF 1958

NASA SCIENTIFIC AND TECHNICAL PUBLICATIONS

TECHNICAL REPORTS: Scientific and technical information considered important, complete, and a lasting contribution to existing knowledge.

TECHNICAL NOTES: Information less broad in scope but nevertheless of importance as a contribution to existing knowledge.

TECHNICAL MEMORANDUMS: Information receiving limited distribution because of preliminary data, security classification, or other reasons.

CONTRACTOR REPORTS: Technical information generated in connection with a NASA contract or grant and released under NASA auspices.

TECHNICAL TRANSLATIONS: Information published in a foreign language considered to merit NASA distribution in English.

TECHNICAL REPRINTS: Information derived from NASA activities and initially published in the form of journal articles.

SPECIAL PUBLICATIONS: Information derived from or of value to NASA activities but not necessarily reporting the results of individual NASA-programmed scientific efforts. Publications include conference proceedings, monographs, data compilations, handbooks, sourcebooks, and special bibliographies.

Details on the availability of these publications may be obtained from:

SCIENTIFIC AND TECHNICAL INFORMATION DIVISION

NATIONAL AERONAUTICS AND SPACE ADMINISTRATION

Washington, D.C. 20546